2012-03

A Mesoscale Model Analysis of Sea Fog Formation and Dissipation Near Kunsan Air Base

DeMarco, Adam W.

Monterey, California. Naval Postgraduate School

NAVAL POSTGRADUATE SCHOOL

MONTEREY, CALIFORNIA

THESIS

A MESOSCALE MODEL ANALYSIS OF SEA FOG FORMATION AND DISSIPATION NEAR KUNSAN AIR BASE

by

Adam W. DeMarco

March 2012

Thesis Advisor:	Qing Wang
Thesis Co-Advisor:	Shouping Wang
Second Reader:	Wendell Nuss

THIS PAGE INTENTIONALLY LEFT BLANK

REPORT DOCUMENTATION PAGE		Form Approved OMB No. 0704–0188

1. AGENCY USE ONLY *(Leave blank)*	2. REPORT DATE March 2012	3. REPORT TYPE AND DATES COVERED Master's Thesis

4. TITLE AND SUBTITLE A Mesoscale Model Analysis of Sea Fog Formation and Dissipation Near Kunsan Air Base	5. FUNDING NUMBERS
6. AUTHOR(S) Adam W. DeMarco	
7. PERFORMING ORGANIZATION NAME(S) AND ADDRESS(ES) Naval Postgraduate School Monterey, CA 93943–5000	8. PERFORMING ORGANIZATION REPORT NUMBER
9. SPONSORING /MONITORING AGENCY NAME(S) AND ADDRESS(ES) N/A	10. SPONSORING/MONITORING AGENCY REPORT NUMBER

11. SUPPLEMENTARY NOTES The views expressed in this thesis are those of the author and do not reflect the official policy or position of the Department of Defense or the U.S. Government. IRB Protocol number _____N/A_____.

12a. DISTRIBUTION / AVAILABILITY STATEMENT Approved for public release; distribution is unlimited	12b. DISTRIBUTION CODE A

13. ABSTRACT (maximum 200 words)

This research used the Coupled Ocean/Atmosphere Mesoscale Prediction System (COAMPS) to examine the physical processes affecting sea fog development near Kunsan AB. The simulated sea fog event occurred from 30 March to 02 April 2011 and was validated using observations. Model results were analyzed from three perspectives. A trajectory analysis examined the evolution of the wind, air-sea interaction, and thermodynamic properties of the air column prior to the sea fog formation; a time variation of similar properties at fixed locations investigated the evolution of the fog for the entire life cycle of the fog event; and a vertical cross-section through Kunsan AB revealed the spatial variability and the effects of coastal circulations. Finally, evaluation of a current forecast tool, Fog Stability Index (FSI), was conducted to determine its adequacy.

Results from this analysis indicated strong influence of the adjacent sea on the fog development and maintenance at Kunsan AB. For the fog event studied in this research, fog initially developed as nocturnal fog over land, but was later maintained by advection from the sea. Strong cooling within the fog layer was present resulting in significant surface-air temperature difference, likely associated with radiation cooling. Radiative cooling, however, did not result in turbulent mixing due to the shallowness of the fog layer and the stable thermal stratification. The presence of the fog layer along the coast appeared to modify the coastal circulation, which was also an important component in introducing moisture into Kunsan AB for fog formation/maintenance. Dissipation of the fog was dominated by synoptic changes. A modified version of FSI is suggested based on results from this study.

14. SUBJECT TERMS Sea fog forecasting, fog stability index, back trajectory analysis, spatial variability, time series analysis, Kunsan AB, and COAMPS mesoscale model	15. NUMBER OF PAGES 97
	16. PRICE CODE

17. SECURITY CLASSIFICATION OF REPORT	18. SECURITY CLASSIFICATION OF THIS PAGE	19. SECURITY CLASSIFICATION OF ABSTRACT	20. LIMITATION OF ABSTRACT
Unclassified	Unclassified	Unclassified	UU

NSN 7540–01–280–5500 Standard Form 298 (Rev. 2–89) Prescribed by ANSI Std. 23918

THIS PAGE INTENTIONALLY LEFT BLANK

Approved for public release; distribution is unlimited

A MESOSCALE MODEL ANALYSIS OF SEA FOG FORMATION AND DISSIPATION NEAR KUNSAN AIR BASE

Adam W. DeMarco
Captain, United States Air Force
B.S., Pennsylvania State University, 2003

Submitted in partial fulfillment of the
requirements for the degree of

MASTER OF SCIENCE IN METEOROLOGY

from the

NAVAL POSTGRADUATE SCHOOL
March 2012

Author: Adam W. DeMarco

Approved by: Qing Wang
Thesis Advisor

Shouping Wang (NRL)
Thesis Co-Advisor

Wendell Nuss
Thesis Second Reader

Wendell Nuss
Chair, Department of Meteorology

THIS PAGE INTENTIONALLY LEFT BLANK

ABSTRACT

This research used the Coupled Ocean/Atmosphere Mesoscale Prediction System (COAMPS) to examine the physical processes affecting sea fog development near Kunsan AB. The simulated sea fog event occurred from 30 March to 02 April 2011 and was validated using observations. Model results were analyzed from three perspectives. A trajectory analysis examined the evolution of the wind, air-sea interaction, and thermodynamic properties of the air column prior to the sea fog formation; a time variation of similar properties at fixed locations investigated the evolution of the fog for the entire life cycle of the fog event; and a vertical cross-section through Kunsan AB revealed the spatial variability and the effects of coastal circulations. Finally, evaluation of a current forecast tool, Fog Stability Index (FSI), was conducted to determine its adequacy.

Results from this analysis indicated strong influence of the adjacent sea on the fog development and maintenance at Kunsan AB. For the fog event studied in this research, fog initially developed as nocturnal fog over land, but was later maintained by advection from the sea. Strong cooling within the fog layer was present resulting in significant surface-air temperature difference, likely associated with radiation cooling. Radiative cooling, however, did not result in turbulent mixing due to the shallowness of the fog layer and the stable thermal stratification. The presence of the fog layer along the coast appeared to modify the coastal circulation, which was also an important component in introducing moisture into Kunsan AB for fog formation/maintenance. Dissipation of the fog was dominated by synoptic changes. A modified version of FSI is suggested based on results from this study.

THIS PAGE INTENTIONALLY LEFT BLANK

TABLE OF CONTENTS

LIST OF FIGURES

THIS PAGE INTENTIONALLY LEFT BLANK

LIST OF TABLES

THIS PAGE INTENTIONALLY LEFT BLANK

LIST OF ACRONYMS AND ABBREVIATIONS

8 OSS/OSW	8th Operations Support Squadron, Weather Flight
AB	air base
AFCCC	Air Force Combat Climatology Center
AFWA	Air Force Weather Agency
BL	boundary layer
CART	classification and regression tree
CCN	cloud condensation nuclei
COAMPS	Coupled Ocean/Atmosphere Mesoscale Prediction System
D	dimension
DPT	dew-point temperature
ECS	East China Sea
F	Fahrenheit
FSI	Fog Stability Index
GMT	Greenwich Mean Time
km	kilometers
kts	knots
LHF	latent heat flux
LL	low level
KST	Korean standard time
m	meters
MABL	marine atmospheric boundary layer
mb	millibars
METARs	Aviation Routine Weather Reports
MVOI	Multivariate Optimum Interpolation
NOGAPS	Navy Operational Global Atmospheric Prediction System
NRL	Naval Research Laboratory
OCDS	Operational Climatic Data Summary
OWS	Operational Weather Squadron

PBL	planetary boundary layer
q_c	cloud mixing ratio
q_v	water vapor mixing ratio
RH	relative humidity
ROK	Republic of Korea
ROKAF	Republic of Korea Air Force
ROT	rule of thumb
SHF	sensible heat flux
SPECIs	Aviation Selected Special Weather Reports
SST	sea surface temperatures
TKE	turbulent kinetic energy
USAF	United States Air Force
USN	United States Navy
UTC	coordinated universal time
WRF	Weather Research and Forecasting
WS	weather squadron
WV	water vapor
YS	Yellow Sea
Z	Zulu time

ACKNOWLEDGMENTS

This process has been the most enjoyable, and at times, the most daunting; however, I have a few people to thank for making it more of the former rather than the latter. Without this person I would not have been able to proceed with some of my ideas. Professor Qing Wang has guided me towards a very structured and coherent path, enabling me to succeed in this endeavor. I thank her for all of her guidance and advice throughout this process.

In addition, I would like to thank the two masterminds behind the COAMPS model data, Dr. Shouping Wang and Ms. Hway-Jen Chen. With their knowledge and expertise on the COAMPS model, they provided me with steadfast results.

Also, I would like to thank Professor Ian Simmonds from The University of Melbourne, Australia, School of Earth Sciences and the math department at the College of Staten Island who provided us with a very useful Lagrangian back trajectory code enabling us to depict the simulation wind in a way that allowed us to view the fog from different vantage points.

Next, I would like to thank my classmates, colleagues, and friends for providing me with insight and ideas on how to proceed when I was in a bind. Their advice and information was definitely appreciated and needed. Also, thank you to members of the 8 OSS/OSW, 17 OWS and the 607 WS for giving me the necessary data and information needed to successfully complete this project. They gave me a great understanding of the environment, Korean Peninsula, in which this thesis was centered around.

Last, but certainly not least, I would like to thank my loving and encouraging family for their constant support throughout this long process. Without them, I would certainly not be as dedicated or motivated. So to say the least, they are why I do what I do. I love you and appreciate all you have done for me. Thank you!

Adam W. DeMarco

THIS PAGE INTENTIONALLY LEFT BLANK

I. INTRODUCTION

A. SEA FOG FORECAST ISSUE AT KUNSAN AIR BASE

Sea fog has always caused havoc throughout the oceans around the world. For many years, this weather phenomenon has plagued United States Air Force (USAF) air bases (ABs) near and around the Republic of Korea (ROK), due to its difficult predictability. Because of its low visibility, aircraft missions have been adversely affected causing ground aborts and, in some cases, inability to complete military operations. For instance, Kunsan AB, ROK (Figure 1) has been dealing with the forecast challenges associated with advection sea fog since the opening of the base in 1938 when Japanese forces, occupying Korea, built a base near the town of Gunsan for fighter-interceptor aircraft. It was not until 1950, when the U.S. recaptured it from the North Koreans during the Korean conflict and decided to make it a permanent AB (GlobalSecurity.org).

Within the last decade, forecasters assigned to the 8th Operations Support Squadron Weather Flight (8 OSS/OSW) along with the 17th Operational Weather Squadron (17 OWS) located at Hickam AB, Hawaii have been struggling with this forecast problem and have requested additional research to be completed to analyze this phenomenon.

In 2004, Capt Danielle Lewis attacked this problem using ten years of surface observations, upstream upper air data, sea surface temperatures (SST) over the Yellow Sea (YS), and data from a 2.5 degree resolution Navy Operational Global Atmospheric Prediction System (NOGAPS) model, along with a classification and regression tree (CART) statistical analysis technique which would help determine predictors of sea fog. The initial outcome of this statistical analysis created forecast guidelines to aid forecasters in predicting the evolution of sea fog events and advection over the area (Lewis 2004). However, with Capt Lewis' research, the 17 OWS (primarily responsible for forecasts throughout the ROK) was unable to produce a useful rule of thumb (ROT) to use for sea fog forecasting. Perhaps the main concern with this approach was her use

of a very coarse resolution model when trying to describe and analyze a mesoscale phenomenon, such as advection sea fog. In addition, a high false alarm rate was identified by using her results during the sea fog season.

It is very difficult for a low resolution model to resolve fog features that are only a few 100 kilometer (km) wide, and at most, 2 km deep. Therefore, with new and improved models and the ability to look at the environment with higher resolution and more accuracy, I have elected to take on this problem again to help improve on this forecast challenge, ultimately saving money, time, and military resources throughout the region.

Figure 1. Map of ROK – red star marks Kunsan AB (After Microsoft 2011; available online at http://www.bing.com/maps/)

The intentions of this research were not to utilize her techniques, but to simply examine a particular fog case by using the Coupled Ocean/Atmosphere Mesoscale Prediction System (COAMPS) model simulation and scrutinize it from under a "microscope" (so to speak) to expose the details of the formation and dissipation processes that are unique to advection sea fog in the YS. Along the way, a description of the physical processes which are critical to advection sea fog development will be shown. This research will also include a thorough examination of some recent studies of sea fog in and around the YS and a discussion of the environmental features around the YS that aid in the development of sea fog. Finally, looking through the life cycle of a specific event of a recent sea fog case based on the COAMPS model simulation from 30 March through 02 April 2011, it will become apparent which critical parameters are key to the development and dissipation of sea fog in the YS.

B. MOTIVATION AND OBJECTIVES

The 17 OWS, along with the 8 OSS/OSW, have been in constant struggle with their inability to accurately forecast sea fog. In fact, I recently spoke to two members of the 17 OWS training flight to determine their current forecast techniques for forecasting sea fog. And here were their responses:

> I talked to several sets of forecasters for Kunsan and found out that they most often look at multispectral satellite imagery to determine whether sea fog is a possibility. If fog shows up (in the satellite imagery) they do an evaluation of current and forecast winds with meteograms, synoptic-scale model charts and occasionally alphanumerics to see if it will roll into the base or not. Other than that, they generally do not appear to use ROTs or any other specific training (Alford 2011, personal communications).

The other correspondence was with a seasoned forecaster for the Korean Peninsula who revealed several teaching documents, a list of variables, Fog Stability Index (FSI), and model output to consider when examining whether or not to forecast sea fog for the region. Here was some additional insight he provided when forecasting sea fog.

> Consider measuring wind direction (more often southerly) and speed. Also, look at the dew point temperature relative to SST. Also, environmental stratification is an important consideration—low level (LL)

> stability to any synoptic forcing. Sea fog is most common from March-July. Strong LL jet (pre-frontal) during this timeframe needs to be considered and position of the sub-tropical ridge is also important. Finally, Air Force Weather Agency's (AFWA) Weather Research and Forecasting (WRF) 2-D (dimension) cloud model is pretty good to use. (Headland 2011, personal communication).

So, as you can see, the forecasters have some indication of what to look for when forecasting for sea fog. However, due to the non-existence of a long term fog evaluation and a high turnover rate of forecasters, this forecasting problem remains a challenge and an improvement to this issue must be obtained from this research.

Even though it is a difficult forecast challenge, with the proper understanding of the physical properties and conditions associated with sea fog, an accurate forecast could be made to predict this event with an adequate lead time. Also, since this event has caused many 'headaches' for entire military operations, to include the forecasters, it is imperative that additional research be conducted. With successful results, the hope is to advance USAF mission capability by improving prediction of the onset of advection sea fog along the ROK by providing many hours of lead time for such events.

Before discussing more details, it is important to understand how the AF views fog and how they define it in their instructions. According to the AF manual, AFMAN 15–111, "Fog is a visible aggregate of minute water particles (droplets) that are based at the earth's surface and reduces the horizontal visibility to less than 5/8 statue miles (1,000 meters (m)) and does not fall to the ground as drizzle or rain." (AFMAN 2009). Therefore, in order for the AF to classify restricted visibility as fog, the observer must not be able to see beyond 1 km. This reduction in visibility is the primary reason for many military operations to come to a standstill and frustrations to grow across in the military community. A vast majority of the flying training areas are in the range of the ominous sea fog, and at anytime, can be adversely affected by the rapid developing sea fog. Therefore, it is the goal of this thesis to take the knowledge that is acquired from this research and apply it to improving the forecasters understanding of sea fog and how they can properly inform the mission planners in order for them to mitigate risk and save time, money, and resources.

The primary focus will be on the development and dissipation of the sea fog throughout the region. This weather event occurs all year round, but is at its peak frequency from March through August due to contrast in air and sea temperature and the high concentration of water vapor (WV) throughout the region. In addition, advection fog encompasses approximately 80 percent of all sea fogs over the YS (Zhou and Du 2010). More specifically, the process which is the most dominant over this region is the cooling of the warm, moist air as it advects northward from the warmer, tropical air during the spring and summer months when the SSTs are still relatively cool. This type of sea fog, referred to as advection cooling fog, mostly occurs when the SST<air temperature and the air temperature drops to at or below the dew-point temperature causing saturation or super-saturation and a surface based cloud to form (Wang 1985). In addition, strong tidal mixing (cold water upwelling) and other air-sea interactions are important factors associated with the formation of advection fog over the YS (Cho *et al.* 2000). These, along with a few other classifications of sea fog, will be described in more detail in later sections.

C. SCOPE OF RESEARCH

The intent of this research is to inform the reader of the details surrounding the formation, maintenance, and dissipation of sea fog. This paper will first review the geographical, climatological, and bathymetric influences surrounding the YS to include, ocean floor depths and seasonal ocean currents and atmospheric conditions. Next, it will describe the physical processes which are critical for the numerous types of sea fog formation by examining past research literature and studies specifically focusing on this region of the world. Thirdly, an explanation of the details of the COAMPS model and why it was chosen for this study will be included. Also, this paper will explain the simulation for the case during a significant sea fog event from 30 March through 02 April 2011 and show how the atmosphere changed as the air advected over the base. Through this simulation, various variable outputs were produced that are considered important for sea fog formation, such as: WV and liquid cloud mixing ratios (q_v and q_c), SST, air temperature, dew-point temperature (DPT), relative humidity (RH), potential

temperature, surface latent heat flux (LHF), surface sensible heat flux (SHF), turbulent kinetic energy (TKE) and wind speed and direction. With these variables being analyzed from numerous locations and along many paths and trajectories, it will soon become apparent what variables lead to the formation and ultimate dissipation of sea fog. From these results, the key ingredients will be broken down to show how the formation and dissipation of sea fog changes over time. Finally, an analysis of the FSI will be conducted to validate the quality and accuracy of the tool with the intent to make any improvements to the index to aid the forecasters in a more accurate forecast for sea fog formation.

II. REGIONAL BACKGROUND AND LITERATURE REVIEW

A. GEOGRAPHICAL AND CLIMATOLOGICAL DESCRIPTION OF THE YELLOW SEA REGION

1. Korean Geography

Kunsan AB, ROK is located on the southwest coast of the Korean Peninsula along the YS only 9 m above sea level. This region is directly surrounded by numerous hills which do not exceed more than 50 m high (Figure 2). Even though this terrain is not very high, isolated clouds can form due to orographic lift through the year. Approximately 50 to 100 miles to the east and north respectively are two extensive mountain ranges which reach maximum altitude of 3,000 feet (GlobalSecurity.org). This type of topography tends to be favorable for advective sea fog to flow over base and get trapped by the terrain to the east and north. Due to Kunsan AB's close proximity to the YS, moisture is readily available throughout the fog season. Also, since the fog season occurs during an increase in precipitation, moisture becomes abundant from the increased rainfall. Another source of moisture for the region comes from the Kum river, which flows from the northeast bringing cool, fresh water into the YS and altering the thermal conditions and salinity concentrations of the YS immediately off the ROK.

In addition to the moisture sources available, cloud condensation nuclei (CCN), which aids in the collection of water vapor and enables the water vapor molecules to easily form liquid water are available throughout the year. CCN play a very important role in the formation of sea fog (Wang 1985). They can be abundant throughout the region due to pollution being advected in from China by Yellow Wind during late winter and early spring. Yellow wind is dust that originates in the Gobi Desert and is carried south by cold fronts that move from the northwest. The dust spreads over Korea and can lower visibility, due to the hazy conditions, for as long as 24 hours. Another source of CCN is generated locally by smoke and ash from burning fields primarily in the late summer and fall (Giese 2004).

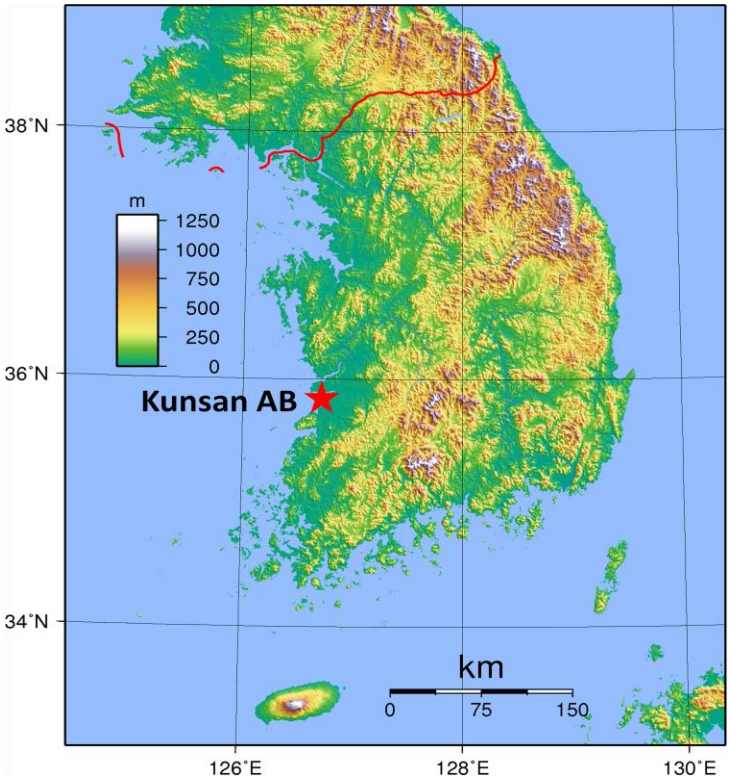

Figure 2. ROK Topography– red star marks Kunsan AB (available online at http://en.wikipedia.org/wiki/File:South_Korea_Topography.png)

2. The Yellow Sea Bathymetry

Another geographic factor that effects the development of sea fog is the bathymetry of the YS. The YS is a shallow sea that lies between northeastern China and the Korean Peninsula, with depths near the center of the sea in excess of 60 to 80 m (Figure 3). The shallowness of the sea leads to variable tidal forcing with peak tidal currents along the shores of southwestern Korea that reach 4.4 $m \cdot s^{-1}$. Like the river runoff, as mentioned in the previous section, strong tidal forcing can lead to variations in the thermal structure and movement of the sea throughout the year making it difficult to predict the SST structure in the proximity of the shoreline. These events contribute to the enhancement of fog development and sustainment and are crucial to understand.

3. Climatology of Atmospheric Conditions of the Region

When forecasting for sea fog it is also important to understand the climatology associated with the ocean currents and the atmospheric synoptic patterns. First, examining the atmospheric climatology for the peak sea fog season (March–August), a main feature that affects the seasonal weather over the ROK is the polar front (Figure 4). This surface polar front, called the Bai-U front, migrates from south of Taiwan in the winter to north of ROK in the summer. The front is formed as cool, moist northeasterly flow from the semipermanent Okhotsk high clashes with the warm, moist southwesterly flow from the Pacific high (Giese 2004). As the front moves north with increased solar radiation over the northern hemisphere, the region experiences its rainy season. When there are variations in the frontal placement and high pressure dominates, foggy conditions likely prevail due to the abundant moisture and warmer air temperatures relative to the SST.

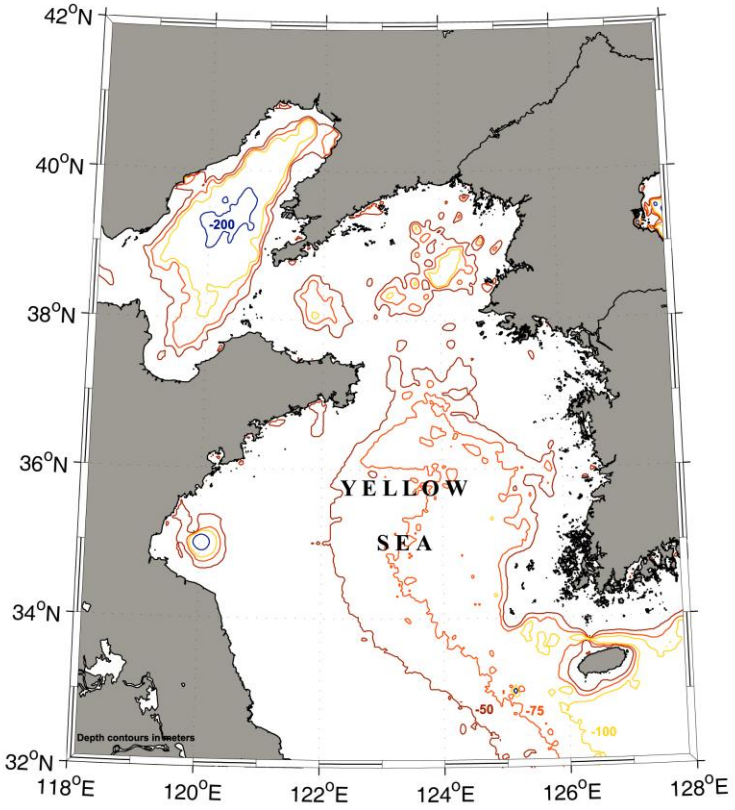

Figure 3. Bathymetry of the Yellow Sea (From Apel 2004)

Table 1 is an excerpt from the Operational Climatic Data Summary (OCDS) for Kunsan AB that shows the seasonal climatology values for surface temperatures, rainfall, mean RH, and surface winds during the fog season. As you might expect, the mean surface temperature increases throughout the season, from the middle 50s in April to the lower 80s by the end of August. Also, because of the northern migration of the polar front and the increase in rainfall, the mean RH increases throughout the period. However, it is important to note that the maximum RH throughout the day occurs during the morning hours at which time Kunsan AB experiences it highest probability of fog, either sea or radiation based. Another interesting fact about the seasonal climatology from the peak sea fog season is the mean surface wind direction. For the majority of the period the winds have a westerly component, which tends to advect in additional moisture off of the YS aiding in the increase in moisture throughout the region.

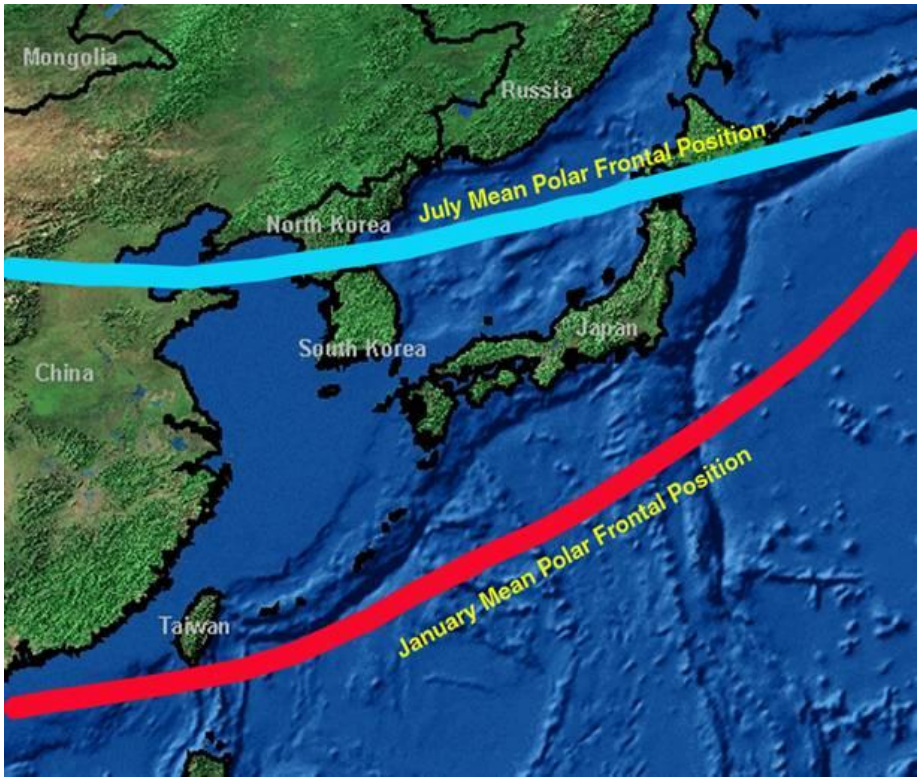

Figure 4. Mean Polar Front Positions (From Giese 2004)

KUNSAN AB CLIMATOLOGY					
Temperature (F)	April	May	June	July	August
Max	59	69	76	83	86
Mean	53	62	70	78	80
Min	46	56	65	74	75
Rainfall (inches)					
Max	9.3	8.6	12.8	22	25.8
Mean	3.8	3.7	5.6	9.9	8.2
Min	0.9	0.4	0.7	2.9	1.1
Mean Relative Humidity (%)					
6 KST (AM)	84	86	88	89	88
14 KST (PM)	65	67	72	76	71
Surface Wind					
Direction	NW	W	W	SW	E
Speed (kts)	10	7	7	9	5

Table 1. Kunsan AB OCDS (After Air Force Combat Climatology Center [AFCCC] 2005)

4. Climatology of the Oceanic Currents in the Yellow Sea

In addition to the atmospheric climatology, the oceanic currents that dominate the region can vary significantly from season to season leading to a more definitive time period of sea fog formation. Specifically, advection cooling fog is closely related to sea currents and their movements (Wang 1985). In addition, tidal mixing is responsible for the cooling of the ocean floor shelf regions in the YS, contributing to a high frequency of sea fog occurrence near the western Korean coast (Zhang *et al.* 2009). So, it is imperative to have a good understanding of the seasonal variations of the currents throughout the YS. The YS undergoes many different current flows throughout the year. In Figure 5, there are some apparent differences between the ocean currents during the summer and winter months. The most dominate oceanic current throughout the region is the Kuroshio current, which brings warm ocean water into the YS as it travels northward at speeds of 0.4 $m \cdot s^{-1}$ or greater (Mask and O'Brien 1998). As the current interacts with the landmasses a number of currents branch off of the Kuroshio and flows out into the Western Pacific, through the Korean Strait, or curves northwestward into the YS.

Within the YS, there are four notable currents that can ultimately affect the ability of sea fog formation. First, the YS Warm Current, with speeds of .25 $m \cdot s^{-1}$, is the main branch of the Kuroshio that provides a warming of the YS throughout the year, but in the summer the current may not penetrate into the YS basin causing less warming to occur. Another significant current is the Korean Coastal Current which travels southward during the year and hugs the west coast of Korea. This cold current is much stronger in the winter, while during the summer it weakens. The YS Coastal Current is another current which dominates the YS in the summer as it travels southward along the Chinese coast. This current joins with the Yangtze River runoff and flows eastward towards the southern tip of the Korean Peninsula. The sea surface that experiences this cold current is usually the forming source of advection cooling fog. More specifically, the regions of warm and cold currents with larger thermal gradients have a greater chance of sea fog formation (Wang 1985). The final region of SST variation occurs in the summer as the river runoff from northeastern China creates a significant pool of cooler water in the central YS region. The YS Cold Water generates tight horizontal sea surface temperature gradients between the warm flowing currents from the south and this cooler pool of water to the north (Mask and O'Brien 1998). The SST gradient that forms during the summer makes it difficult to predict the thermal structure of the YS and the potential formation of sea fog. Also, another factor that makes it difficult to know the SST is the fact that there are few buoy locations in the YS. With the lack of SST observational data, forecasters have a difficult time accurately predicting the SSTs in the YS.

The knowledge of the geography and climatic variations of the YS and the atmosphere throughout the region is key to understanding how the environment will drive the forcing necessary for sea fog formation. In addition to those factors, it is also important to understand the physics behind the formation and dissipation of sea fog.

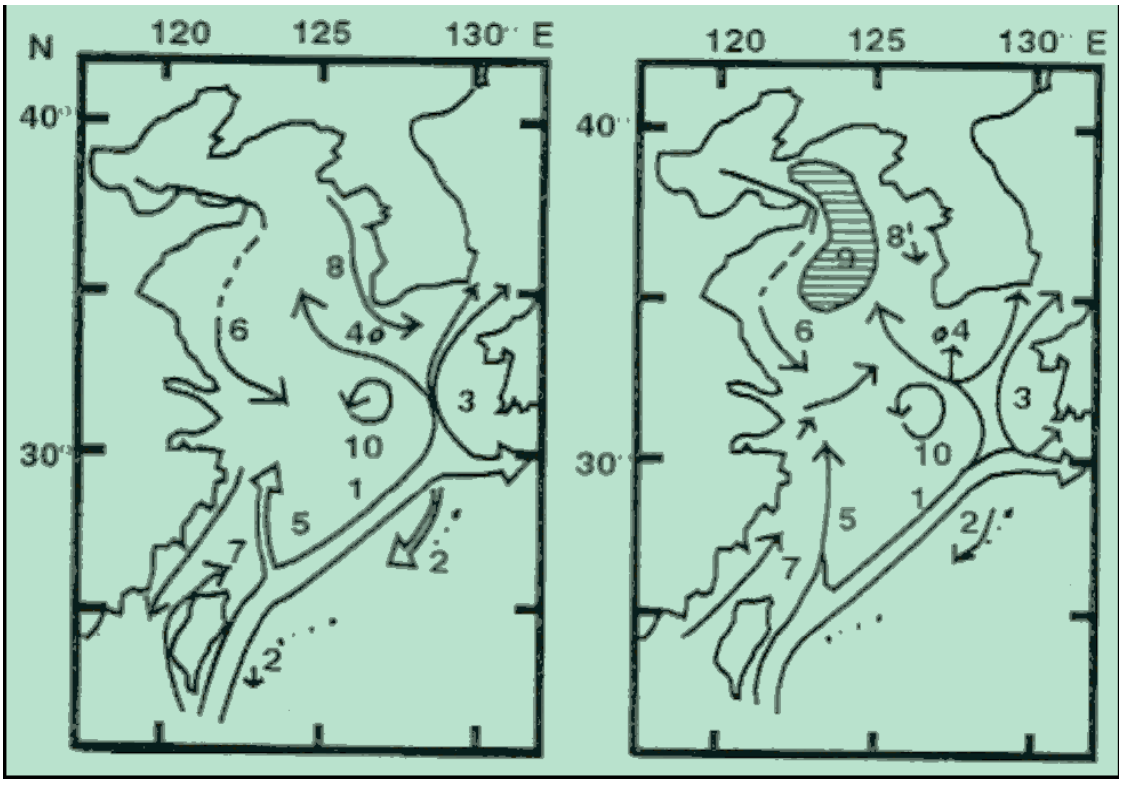

Figure 5. Major currents of the YS region for summer (right) and winter (left). 1, Kuroshio; 2, Kuroshio Countercurrent; 3, Tsushima Warm Current; 4, Yellow Sea Warm Current; 5, Taiwan Warm Current; 6, Yellow Sea Coastal Current; 7, Taiwan Coastal Current; 8, Korean Coastal Current; 9, Yellow Sea Cold Water; and 10, Cheju Cyclonic Gyre. (From Mask and O'Brien 1998)

B. PHYSICS OF SEA FOG AND ITS FORMATION AND DISSIPATION PROPERTIES

There has been numerous research that has focused on sea fog formation and dissipation. One of the most detailed and informative resources came from a book by Wang in 1985, fittingly called "Sea Fog." The work in this field dates back to the 1940s and covers specific details of sea fog in and around the YS. Through his work and experiences, the author classified the different forms of sea fog which develop around the globe (Table 2). However, as we continue, a main focus will be on the advection sea fog processes.

1. Sea Fog Formation Mechanisms

Sea fog can form through two distinct processes related to the immediate surface: surface evaporation and/or cooling. The cooling process occurs under four circumstances: contact, radiation, advection, and cooling induced by turbulent mixing. Contact cooling is when warm air travels over a cooler sea surface and the heat is transferred from air to sea causing the air to cool. This process is normally referred to as turbulent sensible heat transfer. Radiation is the process of radiative energy balance resulting in a net gain/loss of heat at the surface. This process takes into account both the incoming solar radiation and the outgoing long wave radiation to create a net radiation flux resulting in heating or cooling of the ocean surface and eventually causing the temperature change in the lowest level of air adjacent to the surface through turbulent heat exchange. Advection cooling is when cooler air moves over the area. Finally, the turbulence cooling effect transpires when a warm air parcel vertically mixes with a cold air parcel, as if a warm air parcel advectively flows onto a cold water surface and mixes vertically with the cold air staying on the cold surface. These four cooling processes do not occur individually, but are often working together to generate an environment conducive to sea fog formation (Wang 1985).

Basically, in order for sea fog to form the air must increase in moisture content and/or lower in temperature along with having the adequate amount of condensation nuclei available for the water molecules to attach. Once the fog forms, the temperature of the fog drops are further lowered down due to radiation cooling of the fog layer and its boundary. However, for advection cooling fog, not only does the radiation play a role in lowering the temperature of the air, but also turbulence and advection can lead to air temperature cooling. These effects also help to sustain the fog layer over a long period of time. Table 2 shows the breakdown of the sea fog and briefly describes the mechanisms required to form sea fog over various types of oceans and topographical fluctuations (Wang 1985). It is clear from this table that the two main mechanisms for advection sea fog formations are evaporation and cooling.

	Types		Major Cause of Formation
Sea fog	Advection fog	Advection cooling fog	warm air advectively flows onto a cold sea surface
		Advection evaporation fog	cold air advectively flows onto a warm sea surface
	Mixing fog	Cold seasons mixing fog	mixing of cold air with sea surface war-moisture air
		Warm seasons mixing fog	mixing of warm air with sea surface cold-moist air
	Radiation fog	Floating film radiation fog	radiation cooling of floating film of the sea surface
		Salt layer radiation fog	radiation cooling of the salt layer at the top of turbulent layer
		Ice surface radiation fog	radiation cooling of ice surface
	Orographic fog	Island fog	adiabatic cooling of air in windward side of island
		Coastal fog	fog formed in coastal regions

Table 2. Classification of Sea Fog (After Wang 1985)

All of these types of sea fog plague the oceans during various times of the years. However, over the YS, the main culprit for aircraft delays and traffic accidents is due to the advection fog process. This type of fog forms when either warm/cold air flows on cold/warm sea surface, and heat transfers from the air to the sea or from sea to air, respectively. This advective process is also accompanied by a transfer in both SH and LH between the air flowing over the sea. For instance, when SST is less than AT, the SHF from air to sea dominates and causes advection cooling fog to occur. The relationship of air-sea temperature difference that is optimal for advection fog formation is between -0.1°C and 5°C. Therefore, the air temperature must be relatively close to the SST in order for enough cooling to occur for fog formation. While on the other hand, when the SST is greater than air temperature the LHF is significantly enhanced and causes an increase in WV due to the evaporation of the sea surface water. This fog forms because of the increase in WV and is referred to as advection evaporation fog (Wang

1985). A study conducted by Gao *et. al.* 2006 showed a tendency for sea fog formation with a larger air/sea temperature difference and greater wind speeds. It was explained that the stronger the wind shear is, the stronger the resulting mechanical turbulence will be. Therefore, more heat will be transported from air to sea in the stable BL causing favorable environment for sea fog formation. If the air/sea temperature difference is too large then sea fog formation is not as favorable, because the surface buoyancy forcing will generate strong turbulent mixing and hence entrainment of drier air into the BL from above (Gao, *et. al.*, 2006). In terms of the energy exchange and turbulence that occurs between the air-sea, it mainly occurs by the LHF rather than by SHF during an advection fog event. SHF and LHF modified by the SST variations help determine the evolution of sea fog along with changes in the LL static stability. For example, during an advection cooling fog event, an important feature of air and sea coupling happens when the LHF is negative prior to fog formation, which is due to condensation in the stable surface layer (Heo and Ha 2009). Another form of advection fog is referred to as advection-radiation fog. This type of fog occurs along the coastal region and results from the radiative cooling of moist air that has been advected over land from the ocean during the daytime hours (Gultepe *et al.* 2007).

An increase in WV may be due to the air being advected from a source region that has an abundant amount of moisture available and is being carried with flow to a region of less moisture increasing the DPT. For example, when synoptic flow creates a scenario that brings a south to southwesterly wind to the YS region, the area will typically see an increase in RH, which will lead to the increase probability of advection cooling sea fog formation (Heo and Ha 2009). Furthermore, the research has suggested that a heavy frequency of sea fog of more than 50% occurs: 1) in cold water regions that have been generated by strong tidal mixing; 2) when DPT is over 12°C; and 3) DPT minus SST is larger than 2°C (Cho *et al.* 2000). For formation of advection cooling fog, not only does the air temperature need to drop to below the SST, but the DPT should also be at least equal to or higher than the SST. If the water temperature is too high, fog formation is unlikely to occur. Also, sea fog formation is considered favorable when the RH in the region is 90 percent or greater (Wang 1985).

Considering the LWC in the environment is another critically part of the sea fog formation process. In general, as the LWC increases in the air the visibility tends to decrease. For instance, when LWC reaches a minimum of about 0.02 $g \cdot m^{-3}$, the horizontal visibility in fog reaches its maximum at about 1,000 m (the upper limit of fog). Likewise, when the LWC increases up to .85 $g \cdot m^{-3}$, the visibility reduces to about 150 m. Therefore, it is important to consider the amount of LWC in the air to help determine the magnitude of the visibility (Wang 1985). Other considerations for the intensity of the visibility are the density of the fog, which includes the fog drop radius and number of fog drops. This is an inverse relationship where as the number of fog drops decreases with increasing drop radius and vice versa. For example, when the radius of a fog drop is 12 μm the number of fog drops per cubic centimeter had a maximum value well above 100, but the number of drops decreases drastically to less than 10 when the radius was 20 μm (Wang 1985). An additional consideration when looking into the LWC is the variation of LWC in sea fog versus land-based radiation fog. Previous research shows that the LWC in sea fog may be as small as 0.1 $g \cdot m^{-3}$ and as large as 2.0 $g \cdot m^{-3}$, while the LWC for land fog may be as small as 0.01 $g \cdot m^{-3}$ and as large as 1.0 $g \cdot m^{-3}$ (Wang 1985).

In addition to the heat and moisture mechanisms required for advective sea fog formation, an elevated layer of strong thermal stratification capping the LLs is needed. The stable stratification or an inversion primarily occurs under high pressure systems due to adiabatic warming by subsidence. This capping inversion traps the moisture in the LLs. Together will the cooling by radiation, condensation in the layer may occur. Then when the stratification of the LL becomes neutral, the fog layer lifts to become low cloud (Wang 1985). In addition, during a fog event when cooling at the surface increases LL stability, entrainment mixing with the air aloft is reduced. This effect increases the life of the sea fog and generates a horizontal wind speed weaker at the surface. These mechanisms for the formation and sustainment of advection sea fog were discussed in Heo and Ha (2009). In many of the sea fog studies, the average base of the inversion occurred below 200–300 m, which suggests that sea fog events are fairly shallow in depth, but still cause much havoc throughout the aviation industry (Roach 1995).

2. Sea Fog Dissipation Mechanisms

There are a few conditions required in order for dissipation to occur: 1) loss of moisture by precipitation or evaporation; 2) increase in wind speed, specifically when it results in advection of dry air; 3) increase in air temperature; and 4) relaxed LL atmospheric stability. Heo and Ha (2009) found that sea fog dissipated as a result of increased air temperature and reduced moisture due to a decrease in the southerly wind. Other studies also indicated that increasing the wind in fog or introducing charged water droplets generated larger fog droplets and formed drizzle, which led to the dissipation of sea fog. Wang (1985) considered solar radiation as a major cause of fog dissipation. Also, as fog moves over warmer water it will lift into stratus which may later disperse (Roach 1995). Another factor which increases the probability of sea fog dissipation is the coastal diurnal circulation. During the daytime, the sea breeze develops and brings warm and dry air aloft that originated over land. Entrainment of the dryer air from aloft together with daytime shortwave radiative heating of the cloud/fog layers all promote fog dissipation. Finally, as described in the formation section, sea fog is dependent on the thermal structure in the LL. When there is high stability present sea fog is favorable. Likewise, when the LL stability disappears the fog tends to dissipate or transform into low cloud. Koracin *et al.* (2005) concluded that the formation and dissipation of sea fog is closely related to the stratification of air, especially the micrometeorological structure of the LL. In summary, dissipation of sea fog is governed by the complex interplay between advection, synoptic evolution, and development of local circulations

C. SEASONAL SEA FOG VARIATION IN THE YELLOW SEA

As mentioned earlier, advective cooling sea fog can form during any time of the year. However, it develops most frequently during the spring and summer time when the AT>SST and the level of WV is the highest. A study conducted in 2000 by Yang-Ki Cho shows an in-depth analysis of sea fog around the Korean Peninsula and describes the seasonal variation of sea fog in the YS. Figure 6 shows the variations in sea fog rates for the three seas surrounding the Korean Peninsula throughout the year. Clearly, there is a peak in sea fog occurrence (more than 6 days) in the summer, while the average rate of

occurrence of sea fog days are less than one day per month in the autumn and winter. The figure also shows that the most sea fog days occurs twice as frequent in the YS compared to the Sea of Japan to the east of the Korean Peninsula. He concluded that the frequency of sea fog is highly dependent on the difference between the DPT and SST and when it that difference is larger than 2°C. Also, a heavy frequency of sea fog is present under cold water conditions produced by strong tidal mixing, which is partially due to the YS's shallowness, as described in the bathymetry section (Cho *et al.* 2000).

Another important fact to understand regarding sea fog is that unlike other types of fog, sea fog is capable of lasting as long as a few days to weeks at a time, as long as the necessary atmospheric and oceanic conditions persist. For instance, with land-based radiation fog, a typical duration is on the order of hours, because of the diurnal variations due to surface heating and cooling more rapidly. On the other hand, for sea fog the water surface has a much higher heat capacity, so there are very small modifications in the thermal structure throughout the day causing a slower dissipation rate in the liquid water over the ocean.

Another seasonal factor that affects the probability of sea fog formation in the YS is the land-sea temperature difference in the spring (Zhang *et al.* 2009). Because the land warms much more rapidly than the sea when going into the spring season, a strong land-sea thermal difference leads to the formation of a shallow anticyclone over the cool YS and northern East China Sea (ECS). Once this shallow high pressure, and a subsequent LL inversion sets up, the southerly flow on the western part of the anticyclone will tend to advect warm, moist tropical air into the region. As this feature continues, the likelihood of sea fog formation increases abruptly during the spring (Zhang *et al.* 2009).

As described in the section, there are many pieces to this fog forecast puzzle. Therefore, when forecasting for sea fog, it is imperative to understand the mechanisms required for its sustainment and all of the seasonal variations that contribute to the development of this challenging weather phenomena. The next section will discuss the model used for this case study and the specifics of sea fog events that brought havoc to Kunsan AB.

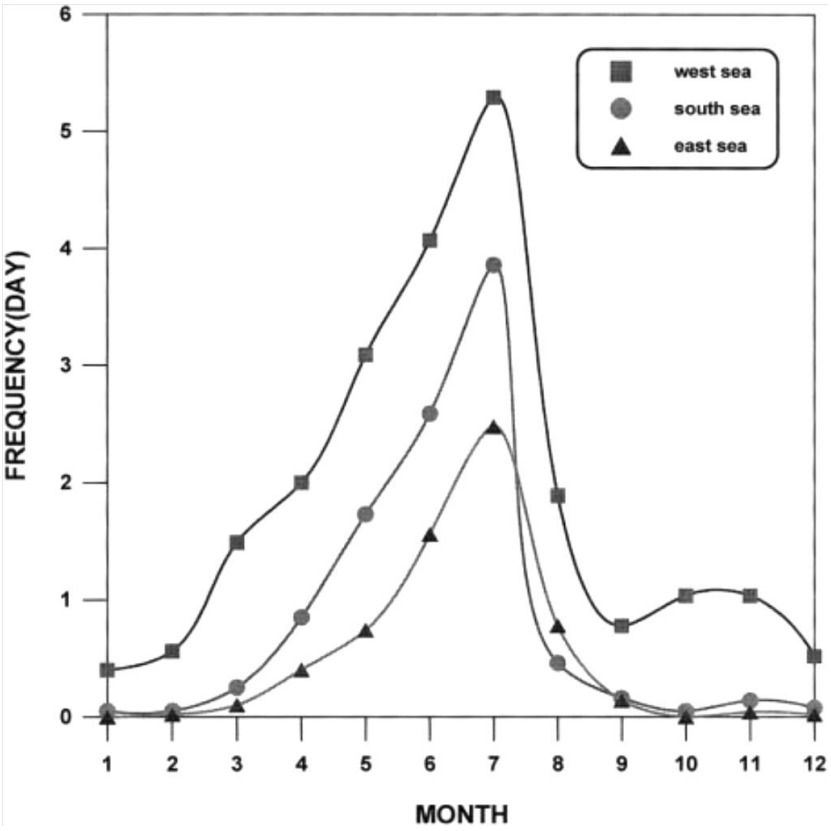

Figure 6. Seasonal variation of mean frequency of sea fog occurrence YS (west sea), Sea of Japan (east sea), and the East China Sea (south sea) (From Cho *et al.* 2000).

III. COAMPS AND COAMPS SIMULATIONS OF FOG EVENTS

A. INTRODUCTION TO COAMPS

One of the many challenges that goes along with forecasting for sea fog is the ability to accurately depict the phenomena using forecast models. The AF uses a non-hydrostatic model called the WRF model which is a mesoscale numerical weather prediction system designed to serve two purposes, both operational and research needs. However, due to the difficulty in obtaining archived model data for this case study, a similar forecast model, COAMPS, was chosen for this simulation.

The COAMPS model (4.2.2 version of the model used in this simulation) was designed by the Naval Research Laboratory (NRL). As the name implies, it couples both atmospheric and oceanic models to provide a more precise representation of the environment and is utilized primarily by the U.S. Navy for operational as well as research use. However, this simulation only used the atmospheric portion of the model to depict the sea fog event due to the limited availability of the coupled model to researchers outside NRL.

The atmospheric component of COAMPS model analysis can use either low resolution model fields from the NOGAPS (cold start) or the most recent COAMPS forecast (warm start) as its first guess of the true atmosphere and use NOGAPS results for its boundary conditions. The analysis also includes a three dimensional Multivariate Optimum Interpolation (MVOI) blend of observational data which is also assimilated with the models first guess field to generate the analysis (NRL 2003). The SST is generated for each forecast by the NRL Coupled Ocean Data Assimilation System (NCODA), which applies a three-dimensional, multivariate, optimum-interpolation method and integrates all available ocean observations in real time, including ship, buoy, and satellite observations as discussed in Cummings (2005).

Like many other forecast models, the COAMPS atmospheric system consists of two major components—analysis and forecast. The analysis, as described above, is run first to generate the initial and boundary conditions for the forecast model. Then the forecast

performs time integrations of the numerics and physics, which then outputs prognostic and diagnostic fields in 3-D coordinates; x, y, and z. In this case, sigma coordinates were used for the z-direction (NRL 2003).

A couple of the important physics parameterizations that were used in this simulation were the Kain-Fritsch moist convection scheme, Harshvardhan radiation module, a slab land surface model, modified Louis surface flux parameterization based on COARE scheme, and Mellor-Yamada Planetary Boundary Layer (PBL) turbulence parameterization. Readers are referred to COAMPS model references (http://www.nrlmry.navy.mil/coamps-web/web/view) and the reference for each physical parameterizations for details of the schemes.

B. OBSERVATIONS OF FOG EVENTS AND CASE SELECTION

1. Kunsan AB METAR Observations

For this case study, it was first necessary to identify a particular period of time when sea fog was present at Kunsan AB to perform a detailed model case study with COAMPS. The primary weather observation system for Kunsan AB is an automated system called the AN/FMQ-19 that automatically produces continuous hourly Aviation Routine Weather. Reports (METARs)/Aviation Selected Special Weather Reports (SPECIs) and is monitored by the 8 OSS/OSW for operational conditions and data accuracy. The Kunsan AB AN/FMQ-19 station is located at 35.92°N/126.62°E, producing METAR/SPECI data of various weather parameters at the surface. The primary weather variables that are displayed on this observation report are as follows: wind speed/direction, visibility, cloud cover/cloud height, present weather type, air temperature, DPT, and altimeter setting (AFMAN 2009). Figure 7 shows a time series of visibilities for Kunsan AB between 30 March and 01 April 2011. The wind barbs are also displayed for the same time period. This figure clearly shows at least three time sections within the time period with decreased visibility to as low as 400 m. These time sections are potential sea fog events impacting Kunsan AB during the three day period. This period was thus selected for COAMPS simulation and extended model data analyses.

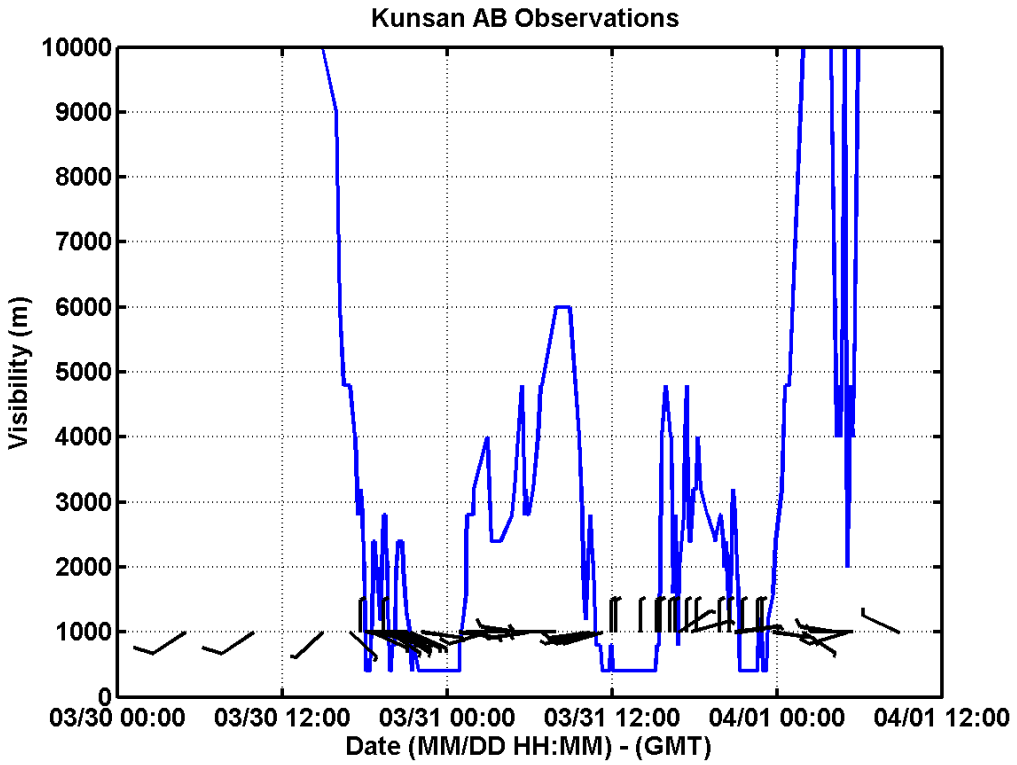

Figure 7. Time series analysis of Kunsan AB's visibility and surface wind bards during the time period of the significant fog event from 30 March - 01 Apr 2011 (visibility less than 1,000 m is classified as fog).

2. Kwangju AB (RKJJ) Upper Air Soundings

In addition to the local METAR observations, upper-air soundings or Skew-Ts were obtained from a Korean AB, Kwangju AB, situated approximately 85 km south-southeast of Kunsan AB. There the local weather unit sends up radiosondes every six hours to measure the atmosphere in the vertical to determine the environmental conditions in the sky directly above the base. Figure 8 gives an example of the Skew-T plot from 31 March/00Z. It shows the presence of extremely low inversion base beneath which the temperature and dew-point temperature are very close in magnitude. This particular sounding seems to indicate saturation (and hence fog) at Kwangju AF at the time of measurements, which was likely the general condition of the southern Korean peninsula. The low visibility observed at Kunsan AB at the same time was thus likely a result of fog.

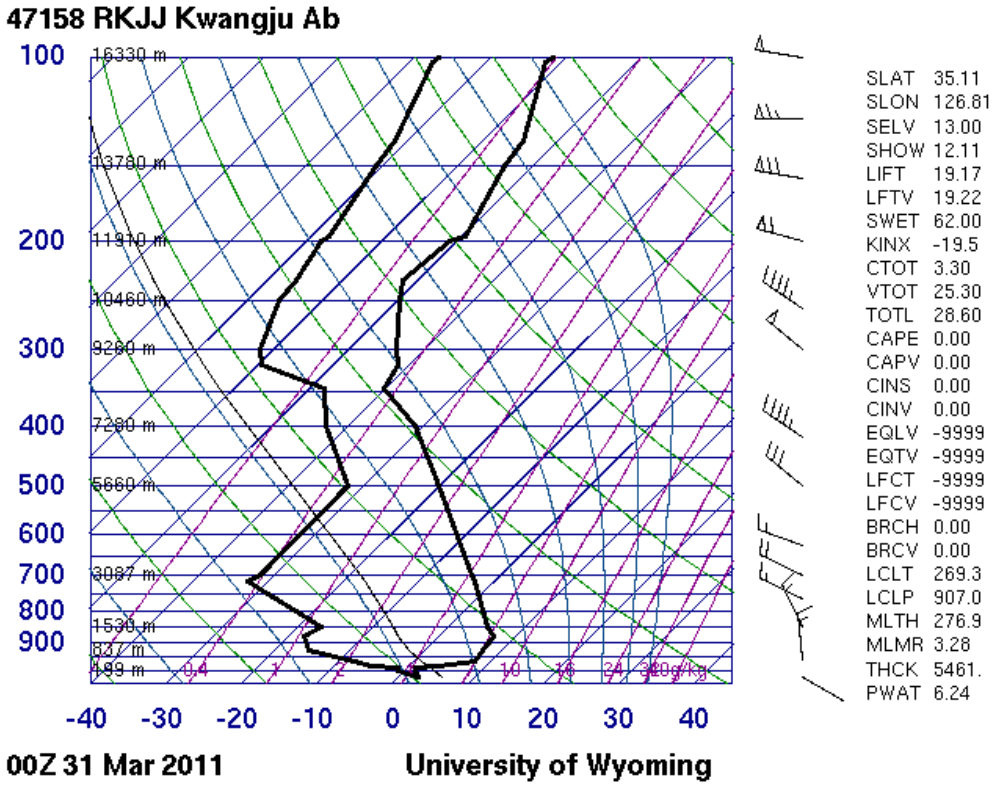

Figure 8. Sounding data for 31Mar/00Z at Kwangju AB. Notice the shallow area of saturation near surface with a very strong LL inversion, which is indicative of fog. (After University of Wyoming at http://weather.uwyo.edu/upperair/sounding.html)

3. Chilbaldo Buoy Station Measurements

Near surface and sea surface conditions were obtained from a buoy station in the YS, called Chilbaldo, approximately 200 km southwest of Kunsan AB. Figure 9 shows the time series of the air temperature, SST, surface pressure, and RH measured from the Chilbaldo buoy for the same time period as in Figure 7. Two time sections were identified where the RH is greater than 90% and the air temperature was cooler than the SST. As described in the previous chapter when the RH is greater than or equal to 90% sea fog formation is favorable. In addition, when air temperature drops to at or below the SST, it is also favorable for sea fog formation. These particular time sections are highlighted in Figure 9, denoting potential sea fog period in the region.

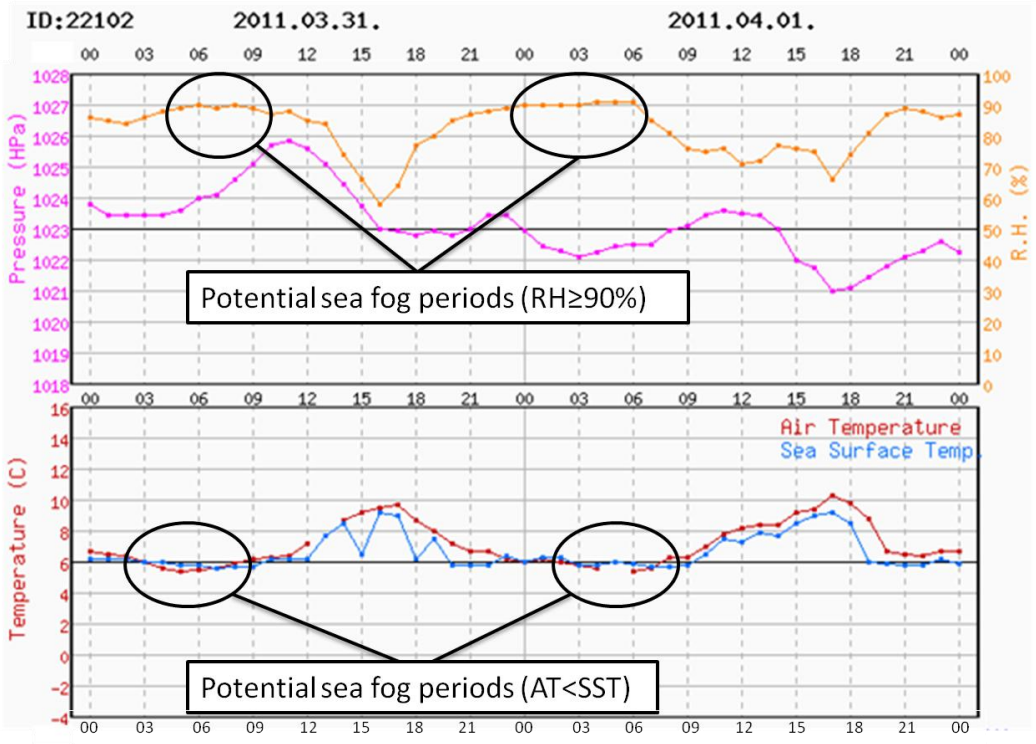

Figure 9. Time series of the buoy data for the buoy station, Chilbaldo from 31 Mar/00KST to 02Apr/00KST. (The circled data shows periods of favorable sea fog formation.) - (After http://www.kma.go.kr/)

4. Regional Satellite Image and Surface Analysis

A satellite cloud image (Figure 10) clearly indicated a sea fog event occurring throughout the west coast of the Korean Peninsula and encompassing a period of approximately two days from 31 March through 02 April. Likewise, the analyzed surface chart (Figure 11), which was generated from the Republic of Korea Air Force (ROKAF), depicts a broad high pressure system draped across the central part of the ECS. This synoptic situation lasted for a few days creating strong subsidence in the mid to lower layers, which led to a strong LL inversion. In addition with the 500 millibars (mb) geostrophic flow from the northwest (Figure 12) and the surface flow from the south-southwest, the wind flow exhibited a clockwise rotation with increasing height. This

veering flow occurs typically with warm air advection. Therefore, with this synoptic set-up, warm air flowed over a cooler underlying surface, the air was cooled below its DPT and fog formation occurred. This synoptic pattern did show formation conditions for sea fog formation.

In summary, based on all the local and regional observations for early spring 2011, it was apparent that a significant low visibility event impacted the region during the period between 30 March to 02 April 2011 period. This time period was the focus of detailed analysis in this thesis study.

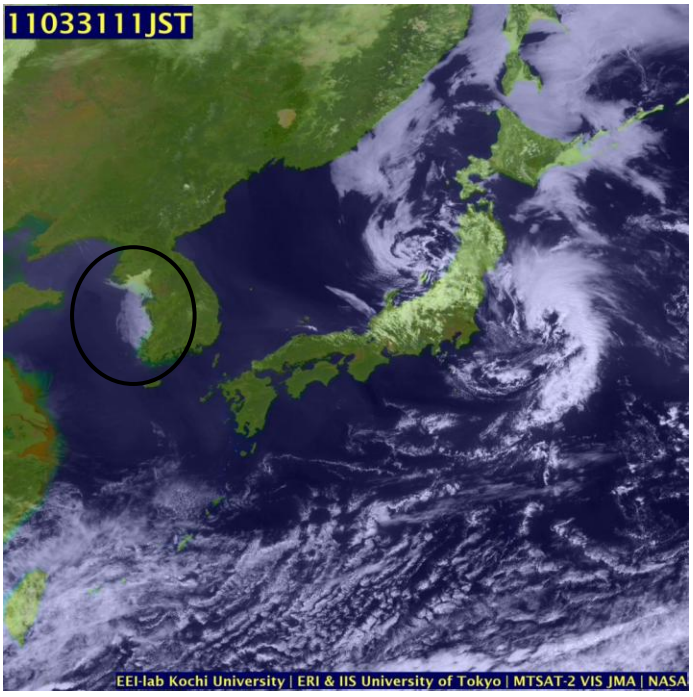

Figure 10. Satellite image of the Korea/Japan region for 31 March/02Z (11 KST). (After http://weather.is.kochi-u.ac.jp/archive-e.html).

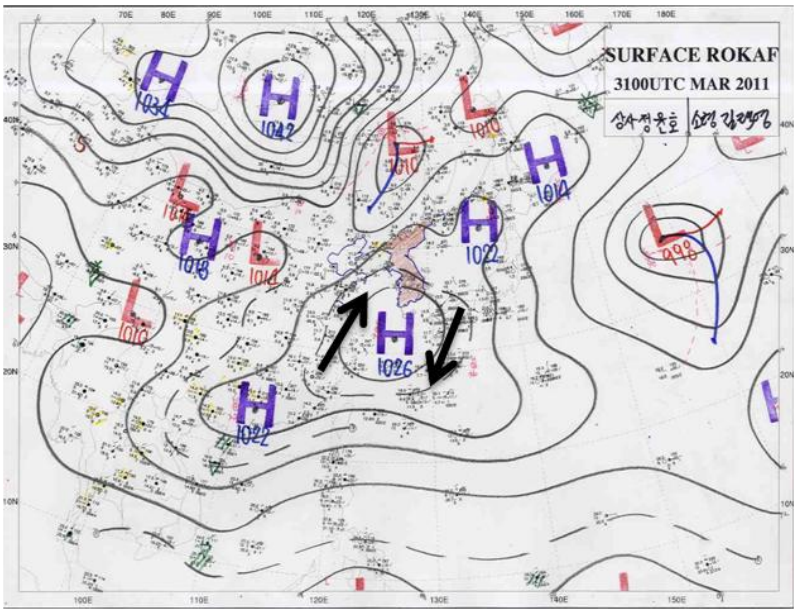

Figure 11. Analyzed surface weather chart for 31 March/00Z with surface wind direction (indicated by bold, black arrows) around the center of the high pressure system over the YS. (After ROKAF 2011)

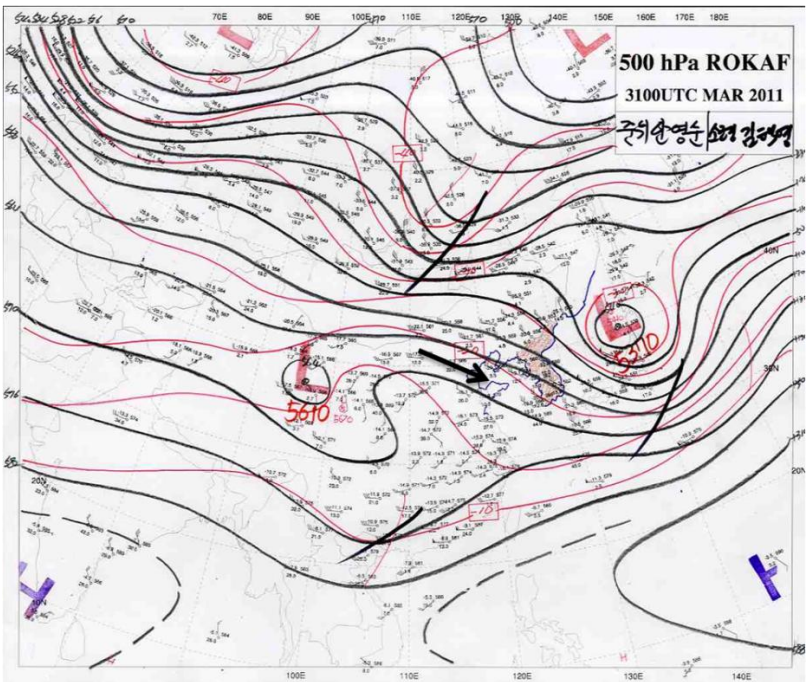

Figure 12. Analyzed 500 mb weather chart for 31 March/00Z with 500 mb flow (indicated by a bold, black arrow) coming out of China into the YS. (After ROKAF 2011)

C. COAMPS MODEL SET-UP FOR KUNSAN FOG SIMULATIONS

1. Model Domain

COAMPS model simulations were made with three-nested model domain within the region of interest. The boxes in Figure 13 represent the area coverage of each domain. The innermost domain was used as the primary source of data for later analyses with the highest grid resolution of 3 km. Also, vertical grid spacing was created using sigma coordinates for 30 different levels extending from 10 m to 31,050 m above the terrain (NRL 2003). However, since the fog in the YS region typically occurs only 1 km or less above the surface, only the lowest 11 sigma levels, with a max height of 1600 m, were used in the analyses. This fine, horizontal and vertical, resolution allows for a more detailed representation of the atmosphere and may contain mesoscale features that are difficult to represent using a lower resolution model, such as in the case of Lewis (2004), where a 2.5 x 2.5 degree grid-resolution model output was used to analyze sea fog events.

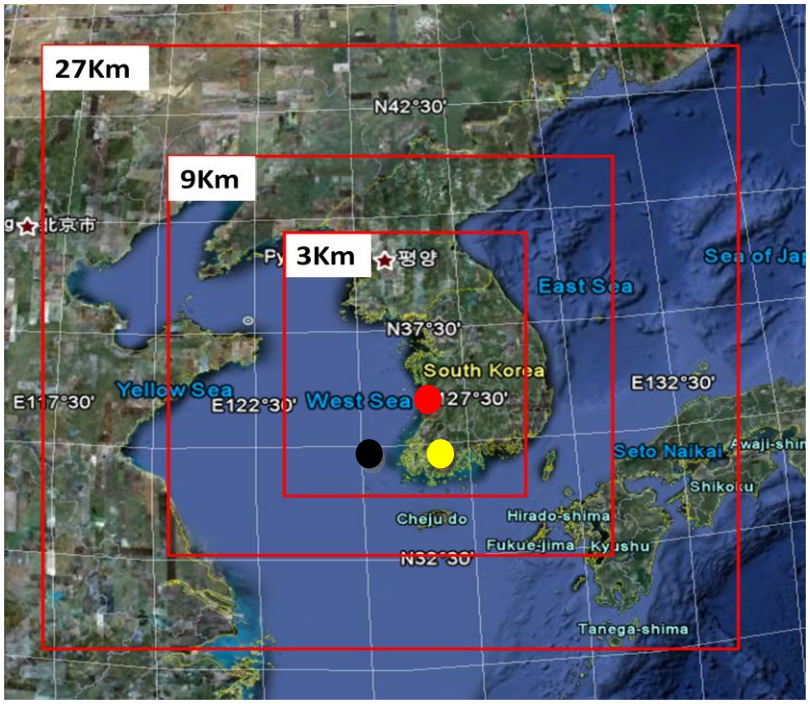

Figure 13. COAMPS model domains (red boxes) and grid spacing used for sea fog case study. Kunsan AB, the Chilbadao buoy station, and Kwangju AB are denoted by the red, black, and yellow dots, respectively.

2. Simulation Setup and Model Output

Each COAMPS forecast run was made for 48-hour periods and a new forecast run was made every 12 hours with updated boundary conditions and the MVOI blend of observational data for data assimilation. The model also ran off the coordinated universal time (UTC) or Zulu time (Z), which is minus nine hours to Korean Standard Time (KST). For the period of interest to this thesis, there were a total of six COAMPS runs, each with a simulation period illustrated in Figure 14. For each COAMPS run, hourly output of mean variables were saved including variables such as pressure, temperature, wind components, q_v, q_c, and so on. We also outputted near surface turbulent quantities such as, surface sensible and latent heat fluxes, TKE and boundary layer height.

Because the model was initialized with new data for each forecast, initial adjustment time was needed for the simulations to reach consistency between the predicted variables and the dynamics. This adjustment usually happens in the first 5–6 hours of the simulation. Also, model error can occur at the end of model runs because the model tends to be less accurate the further out it goes, which can occur after 17 hours of model simulation. Therefore, for these analyses, the forecast results were generated between hour 6 an hour 17 only from each of the forecast run and pieced together to form a continuous time series between 30 March/06Z and 02 April/05Z. Figure 14 shows a schematic of the time period from each forecast to make up the 'best forecast' composite model time series.

For the model output, specific variables were chosen for depicting the atmospheric and oceanic conditions for this sea fog event. When examining a coastal environment it is essential to characterize both the atmosphere and the ocean conditions to understand the air-sea interaction processes involved in fog development processes. Table 3 shows a list of the variables used in this study with the corresponding COAMPS nomenclature and whether or not it is a surface based (2-D) or a 3-D output. Also included in the table are variables derived in post-processing.

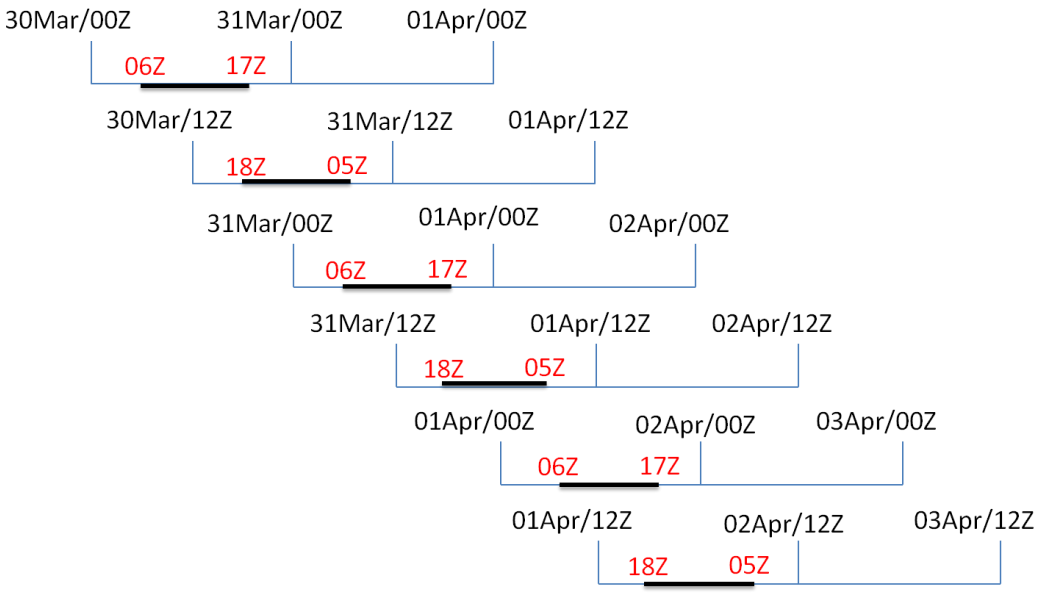

Figure 14. Forecast period of each of the six COAMPS simulations and the "best forecast" time that represents the most accurate period from each model run (the thick black lines). Forecast from all the 'best forecast' period from the time series of COAMPS simulations to be used in the analyses (30 Mar/06Z to 02 Apr/05Z).

Variable	**units**	**COAMPS name**	**levels**
Air Temperature*	C		3D
Cloud Mixing Ratio	$g \cdot kg^{-1}$	cldmix	3D
Dewpoint Temperature*	C		3D
Latent Heat Flux	$W \cdot m^{-2}$	lahflx	2D Surface
Planetary Boundary Layer	m	pblzht	2D
Potential Temperature	K	pottmp	3D
Relative Humidity*	%		3D
Sea Surface Temperature	C	seatmp	2D Surface
Sensible Heat Flux	$W \cdot m^{-2}$	sehflx	2D Surface
Turbulent Kinetic Energy	$m^2 \cdot s^{-2}$	turbke	3D
U-Component Wind	$m \cdot s^{-1}$	uuwind	3D
V-Component Wind	$m \cdot s^{-1}$	vvwind	3D
Water Vapor Mixing Ratio	$g \cdot kg^{-1}$	wvapor	3D
Wind Barb*	kts		3D

Table 3. Variables used in the analyses and their corresponding units, names in COAMPS output, and output levels. The * denotes variables calculated from other direct outputs.

IV. RESULTS

A. SIMULATED FOG EVENT AND MODEL VALIDATION

1. Simulated Fog Formation in the Model Domain

The model simulation produced q_c as an direct output. While this variable denotes the amount of cloud water in the air, it does not directly represent the presence of fog which is defined as visibility being less than 1 km (AFMAN 2009). Therefore, when comparing cloud liquid water content (LWC) to visibility, formulations are needed to convert LWC to visibility limitations to determine fog. Kunkel (1984) discussed this conversion through an extinction coefficient (β):

$$\beta = \pi \sum_{i=1}^{N} Q_{ext}\, n_i\, r_i^2$$

where Q_{ext} is the normalized extinction cross section, and n_i is the number density for cloud droplets of radius r_i. Since cloud microphysics information are not always available in forecast models, Kunkel (1984) further provided an empirical relationship between the liquid water content (LWC) and the extinction coefficient (β):

$$\beta = 144.7(LWC)^{0.88}$$

where LWC is in $g \cdot m^{-3}$. This β can then be translated into visibility:

$$VIS = -\ln(\eta)/\beta$$

where η is the threshold of contrast normally taken as 0.02.

From these empirical relationships it can be determined that when LWC > 0.02 $g \cdot m^{-3}$ visibility is less than 1 km and thus can be classified as fog (Kunkel 1984). Since the air density is close to 1 $kg \cdot m^{-3}$, the threshold of fog for LWC at 0.02 $g \cdot m^{-3}$ is equivalent to q_c at 0.02 $g \cdot kg^{-1}$, which was used as the threshold for fog identification in this study.

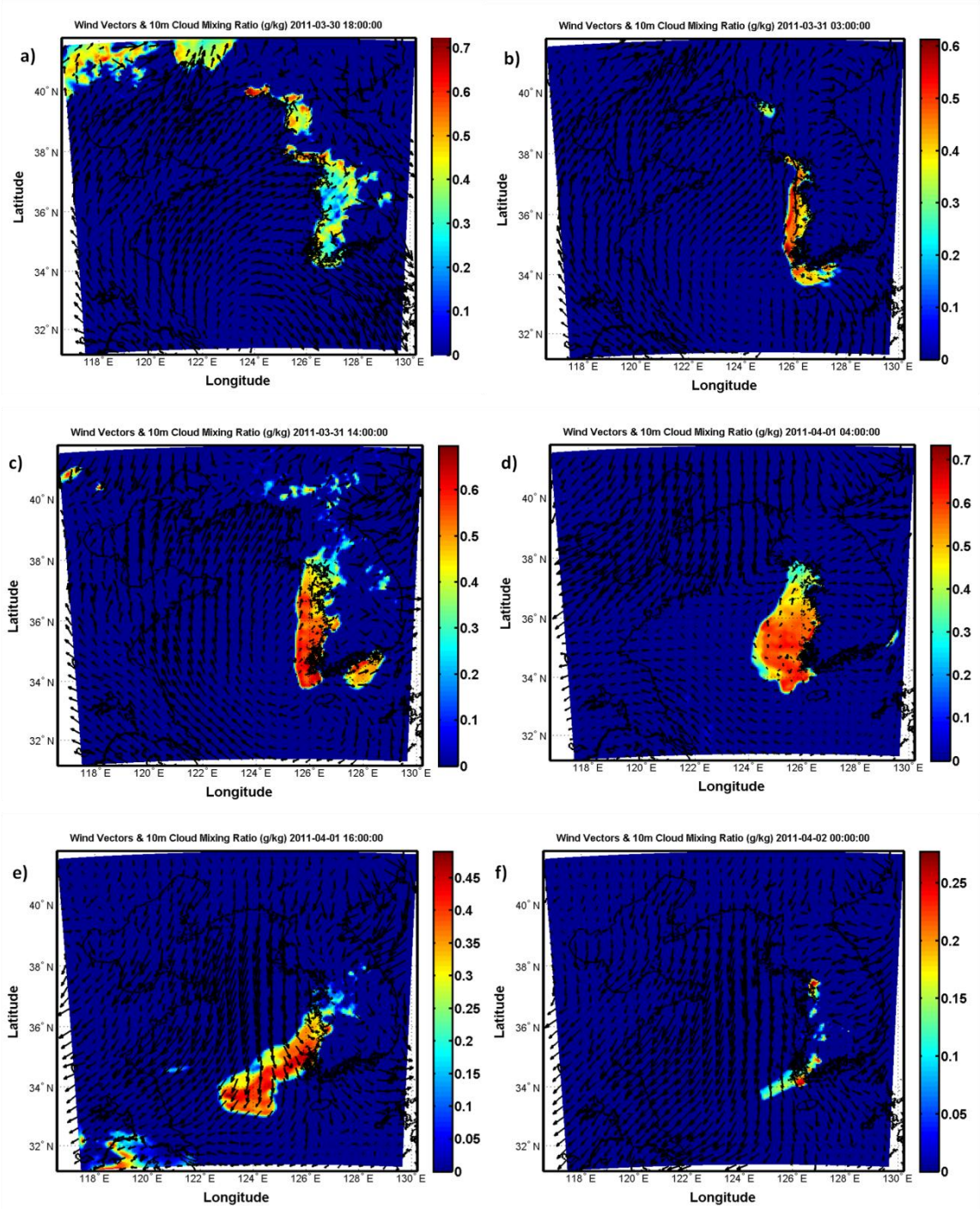

Figure 15. 2-D 10 m q_c. (a-f) shows q_c (colored contours) at selected times to illustrate fog evolution from formation through dissipation in the area of interest. The color bar indicates the magnitude of q_c. The black arrows show the 10 m wind speed and direction with the length of the arrow indicating the magnitude of the winds. Time of results is shown in the title of each figure.

Figure 15 shows a six panel horizontal distribution of the 10 m q_c. Based on the discussions above, colors brighter than dark blue are equivalent to visibility less than 1 km, or fog. Figure 15b at 31 March/03Z is about 1 hour ahead of the satellite image in Figure 10. These two figures show similar region of fog coverage, suggesting a high level of confidence in the model results.

The left panels of Figure 15 show the nighttime fog distribution while the right side panels show the daytime results. From these figures, it appears that the initial fog formed over nighttime land surfaces only, suggesting a radiation fog type. However, later simulations indicated sea fog only without significant fog over land except in the coastal zone. It also appears that the fog began to dissipate (Figure 15e) as northerly wind increased that brought drier air into the region creating less favorable conditions for fog. These developments of fog at different locations will be discussed in further detail in the later sections.

2. Validation of Fog Forecast at Kunsan

In addition to the 2-D q_c plots, time series analyses were conducted over three specific locations. Those locations were chosen carefully to depict the environment over the land, over the sea and along the coast. Figure 16a shows the points of interest and the subsequent q_c values for those locations during the forecast time period (Figures 16b-d). Notice that the Kunsan and land points (Figures 16c & d) show diurnal variations as the level of q_c increased during the night and decreased during the day as the land warmed. While the ocean point (Figure 16b) shows a continuous level of relatively high q_c.

Figure 16c shows the comparison between q_c and the observed visibility (also presented in Figure 7) at Kunsan AB. It is seen that the simulated high cloud water content corresponds well with the observed visibility lower than 1 km (the dash blue line) and hence provides further confidence of the simulated results regarding the presence of fog. However, beyond hour 45 the correlation between the observed visibility and q_c is low. This discrepancy was likely due to the dominance in cloud-top radiative cooling maintaining the fog layer for a long period of time. When comparing the Kunsan and land points time series with the visibility time series from Kunsan AB (Figure 7), there

are very similar characteristics in the fog at the two sites. The q_c at both Kunsan and the land point show diurnal variations in the fog. This suggests that the fog had some interesting variations between the ocean and land surfaces. More details from this simulation will be explored in further sections, however, it is important to note that the simulation does paint an accurate picture of the fog, other than after hour 45 when q_c is continued over Kunsan AB. Therefore, when proceeding with this report the model data will be able to represent the environment accurately.

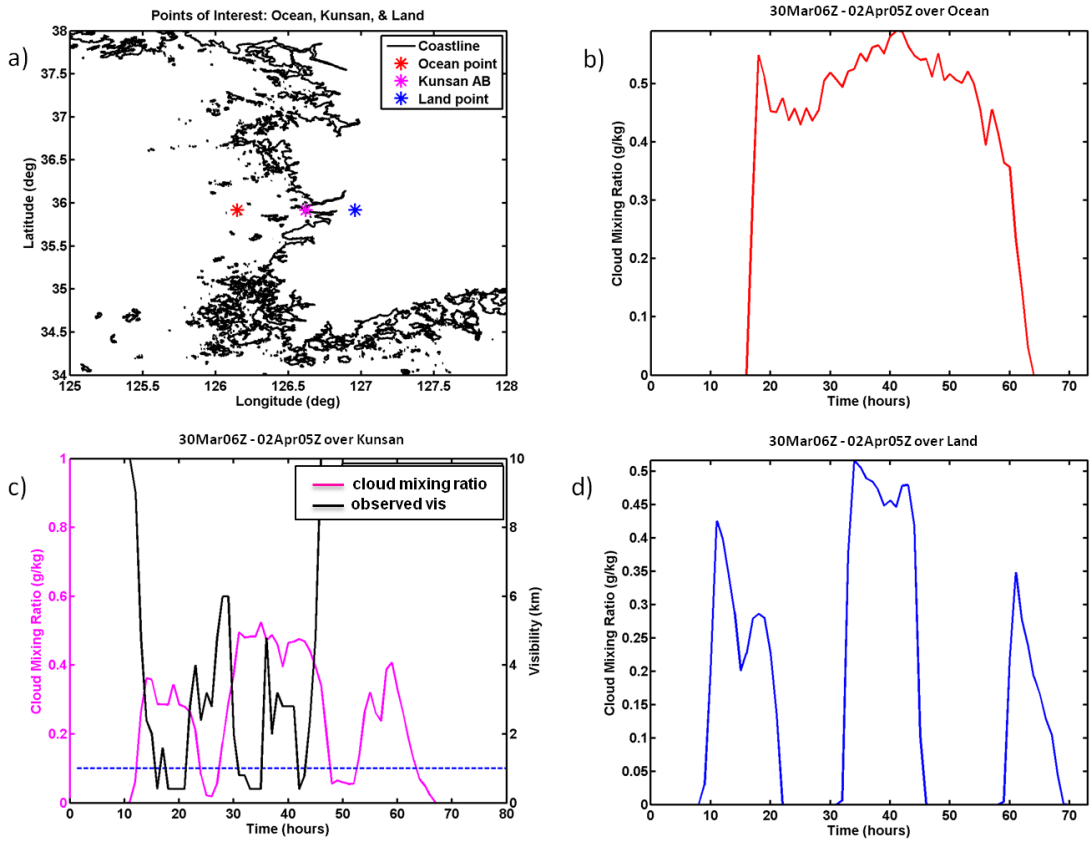

Figure 16. Points of interest for the time series q_c plots. a) the location of the points. b) - d) the variation in q_c from 30 Mar/06Z - 2 Apr/05Z at those specific points. c) compares the q_c for Kunsan to the surface visibility report from the automated sensor with dashed blue line indicating the fog threshold.

B. BOUNDARY LAYER EVOLUTION LEADING TO FOG FORMATION

In order to identify the air mass modification as it moved across the YS, column back trajectories were generated using COAMPS simulated wind fields to show the fog development from the start of the forecast time until the onset of fog at each point of interest. The back trajectory takes into account the 10 m wind speed and direction to determine the location of the air parcel from a starting point and works backwards to obtain the origin of the advected air (Noone and Simmonds 1999). This approach for analyzing sea fog has been used in the past. Koracin, *et al.* (2005) used a model simulation with back trajectory analysis to study sea fog along the California coast. They concluded that it was crucial to investigate the formation, evolution, and dissipation of sea fog in a Lagrangian framework using back trajectory, both over water and land (Koracin *et al.* 2005).

In this study, three locations were chosen for this analysis, including one ocean point (point O), one land point (point L), and the central point at Kunsan AB. The starting points for the trajectories were determined based on the approximate time fog formed at the given points. Comparison among the three locations revealed the difference in land and sea surfaces that contributed to the variations of fog development throughout the region. Analysis from these three points enabled for a detailed description of the fog/non-fog environment over the ocean and over land. Figure 17 shows the three points on the map with the corresponding back trajectory, each trajectory started at the onset of fog of the corresponding location. The location and the time period for trajectory calculations are given in Table 4.

	Ocean (point O)	**Kunsan AB**	**Land (point L)**
Latitude	35.92°N	35.92°N	35.92°N
Longitude	126.15°E	126.62°E	126.96°E
Time Period	30 March 22Z - 10Z	30 March 18Z - 06Z	30 March 15Z - 06Z

Table 4. Location destination and time period for back trajectory analyses based on COAMPS forecast winds. The ocean and the land points will be referred to as point O and L, respectively.

The first, and most obvious, feature that stood out on Figure 17 were the westerly direction of all three trajectories, which suggested air flow of ocean origin. In addition, the wind field indicated modest that averaged about 4.6 $m \cdot s^{-1}$ from west-southwest. Analyses of various physical parameters along these trajectories are given in the following subsections.

Using the trajectories to examine the air flow prior to the fog formation at three locations is an important step in understanding the processes that are key in advection sea fog formation. The trajectories not only tell us where the air originated and its properties but also show us how the air evolved along the trajectory path. Therefore, it was necessary to dissect these model output variables by looking at each along its path. For clear understanding, the back trajectory results will be discussed in a forward trajectory sense to represent the actual forward path the air took prior to the fog formation. All variables showed significant variations along the trajectory. In particular, the LHF and SHF showed some major differences as the air column moved from ocean to land surfaces.

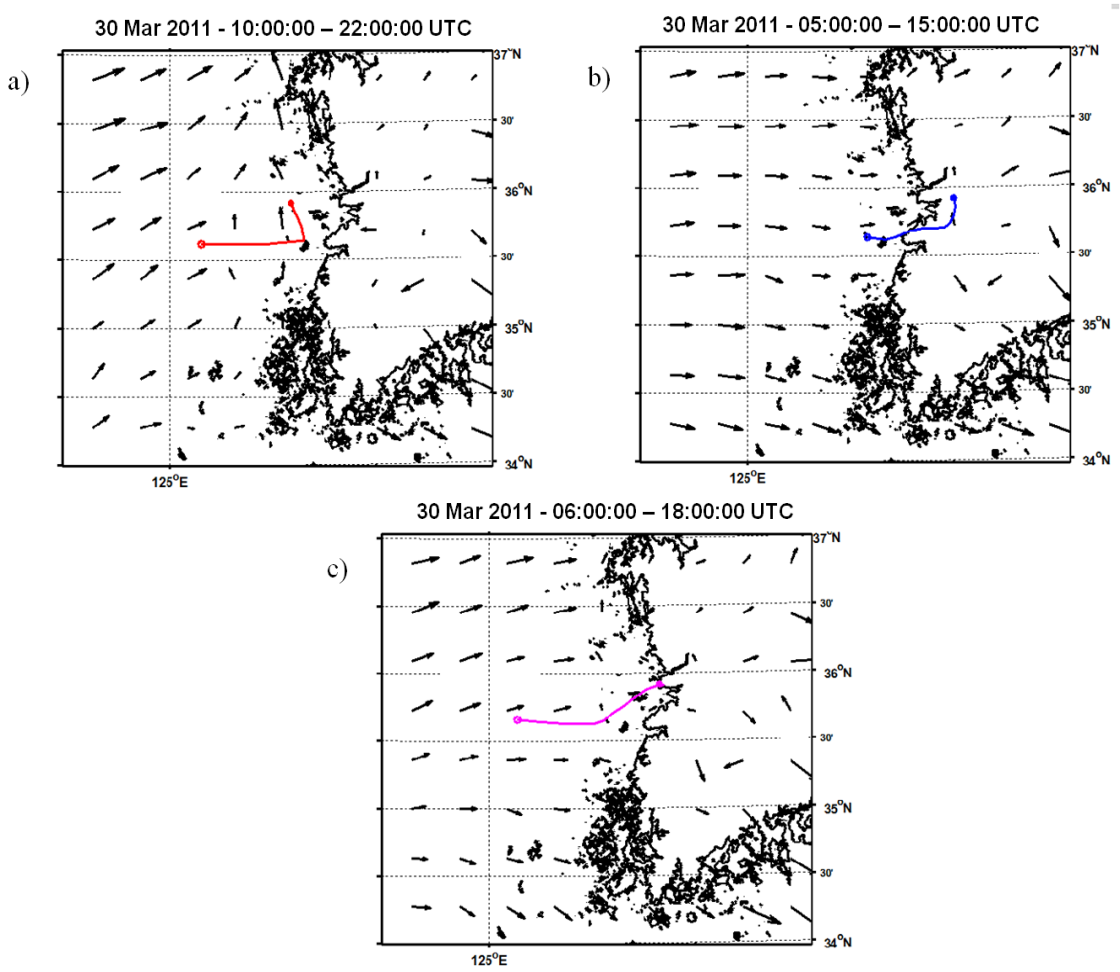

Figure 17. Back trajectory from start of fog at each point. a) point O, b) point L, c) Kunsan. The arrows represent the wind vectors at 10 m above the surface at the start of the fog. (After University of Melbourne at http://www.earthsci.unimelb.edu.au/trajectories/trajhome.htm, Noon and Simmonds 1999).

1. Coastal Ocean Location

Figure 18 shows a point by point map of the forward trajectory, beginning with the starting point of the trajectory path (red star) and ending at the point of interest (yellow star) when the fog began. The other points along the path represent the data points every one hour as the air flowed from west to east. The spacing of the data points depict the speed of the flow with larger spacing indicating stronger wind and vice versa. This path was used to show both the changes in the surface variables along with the boundary layer (BL) variables in a vertical contour plot. An interesting observation regarding the first trajectory was the abrupt turn the parcel of air takes prior to fog formation. This change in the wind direction was due to several possible reasons which will be explored later.

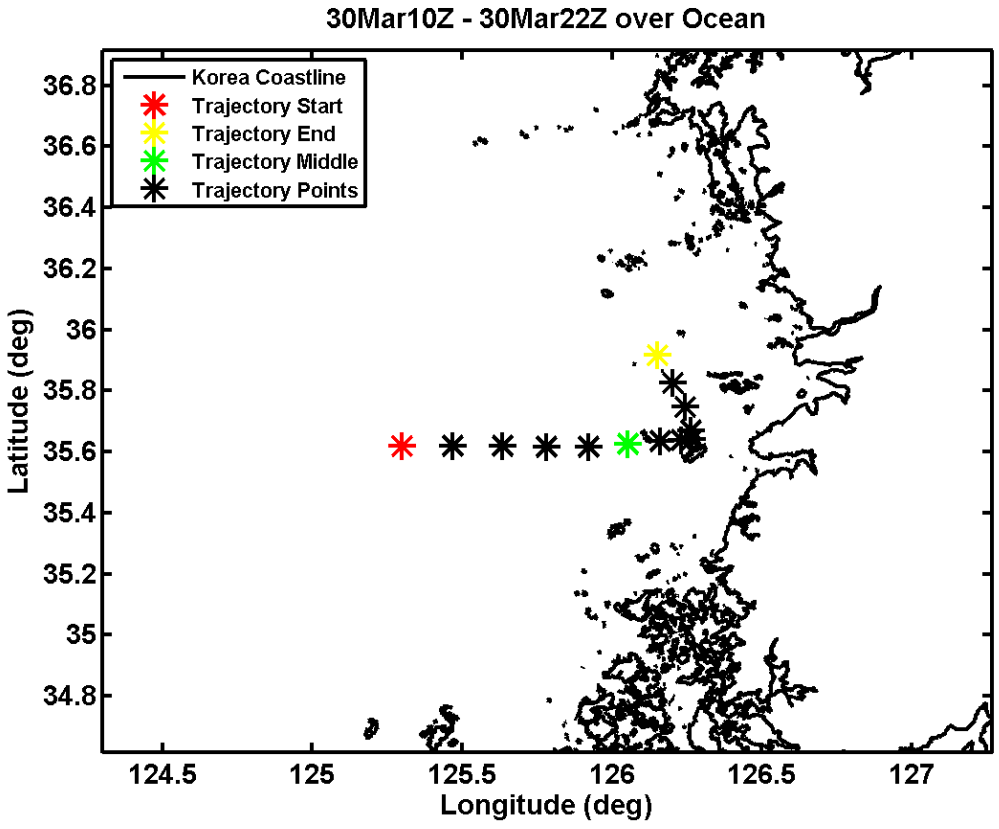

Figure 18. Point O - The trajectory of the air column beginning to the west (red star) and ending at the point of interest when the fog began (yellow star).

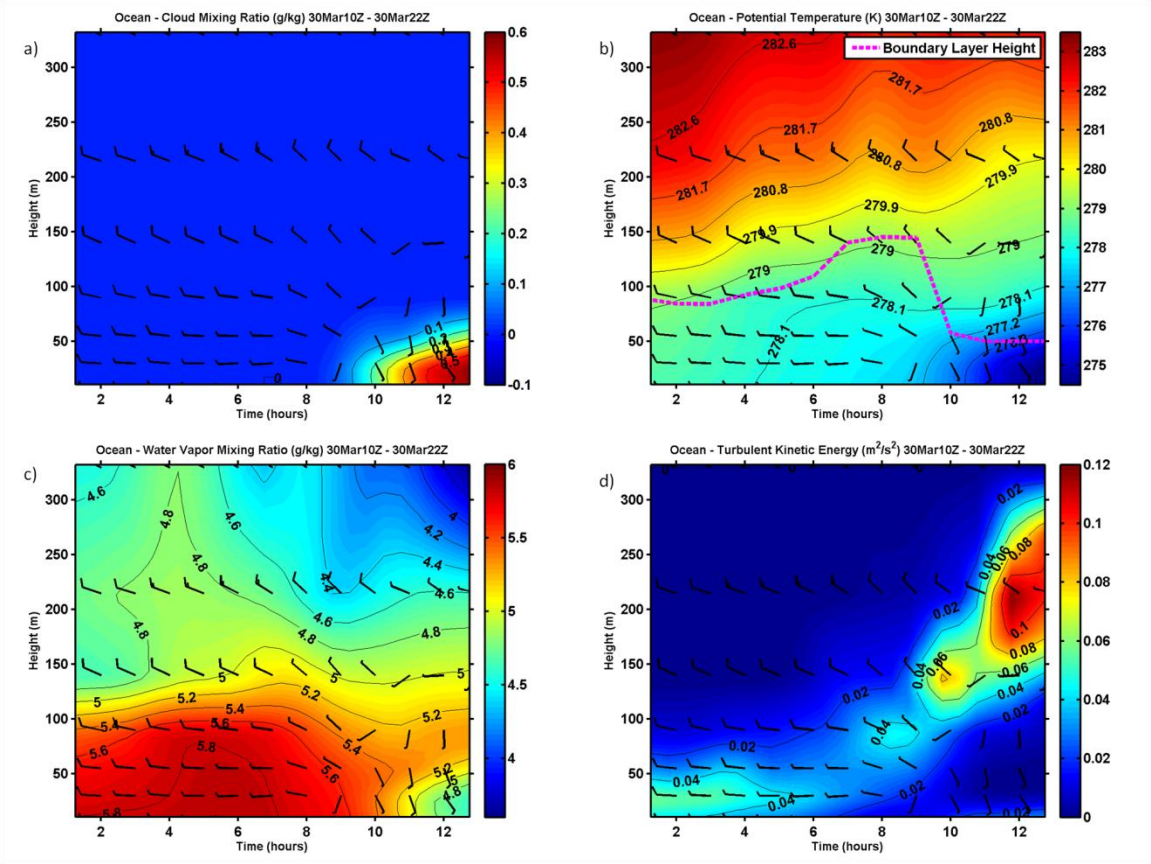

Figure 19. Vertical cross-section plots along the trajectory ending at point O from 30 March/10Z to 30 March/22Z. a) q_c; b) potential temperature with BL height; c) q_v; d) TKE. Wind barbs represent the wind speed and direction of the flow in knots.

Figure 19 shows the vertical cross-section for four variables along the path with wind barbs at multiple levels. The dominate flow in the first 6 hours was westerly during which q_v increased gradually to about 6 $g \cdot kg^{-1}$ (Figure 19c) prior to the fog formation. The start of the fog in the YS is represented by the increase in q_c (Figure 19a) approximately at 19Z or hour 9 from the start of the trajectory. Simultaneously, q_v dropped to below 5 $g \cdot kg^{-1}$ making the total water (the sum of q_v and q_c) the same. The decrease in q_v is consistent throughout the simulation when the fog formed and shows the conversion from vapor to liquid water within the BL.

Through the first eight to nine hours of the trajectory, potential temperature (Figure 19c) of the marine atmospheric boundary layer (MABL) was fairly well mixed

with an increase in static stability as fog formed in the air column. Once fog formed, the lower layer became stably stratified up to 100 m topped by a weakly stratified layer above. The fog layer also experienced a fairly rapid decrease in temperature from 278K to 275K in the next 4 hours. This decrease in temperature is likely caused by cloud-top radiative cooling. Koracin, *et al.* (2005) showed their modeling results had identified radiative cooling as a major determinant of MABL cooling. Their scale analysis showed that the radiative cooling term in the thermodynamic equation dominated the surface SHF and LHF, and entrainment terms along the modified path of the air trajectory in and around the fog layer (Koracin *et al*. 2005). Further results from this study also showed the dominant effect of cloud-top radiative cooling in the simulated fog event on the thermal structure of the MABL.

Examining the surface forcings and temperature of the air in the LL marine environment was another important part for identifying the mechanisms responsible for the formation of the sea fog. Figure 20 shows comparisons of atmospheric and oceanic variables that supported the development of advection fog. As the air parcel progressed eastward, the 10 m air temperature began to decrease due to the heat exchange with the cooler SST (Figure 20c). As fog formed, the air temperature continued to drop by 3°C in a 3 hour period. This significant drop in 10 m air temperature was in part due to the dominate radiative cooling in the model, as described above. In addition, according to Wang (1985) it is necessary for the dew-point temperature and the air temperature to be higher than the SST in order for condensation to occur (Wang 1985). When comparing the three temperatures (Figure 20a/c) to the start of the fog (Figure 20d), it appears that the 10 m air and dew-point temperatures were higher than the SST right at the start of the fog. However, it was not until the SST dropped to below 6°C that the dew-point temperature became larger than the SST. Then within one hour of the temperatures meeting these conditions the fog formed. Also, when the fog formed between 18Z and 19Z, the 10 m dew-point and air temperature became the same, indicating saturation. At that point, the q_v decreased from 6 to 5 $g \cdot kg^{-1}$ as the water molecules converted from gas to liquid form (Figure 20d).

The SHF and LHF (Figure 20b) shows the SHF being slightly negative prior to the fog formation. The negative surface SHF was consistent with the warmer air over the cooler sea surface causing the heat to be transported downward from air to sea. Also, the LHF was only slightly positive prior to the fog meaning the saturated sea surface was supplying the air with moisture. The weak LHF is also indicative of surface air being near saturation. Then when the fog formed both the SHF and LHF began to increase rapidly, because the rapid decrease in air temperature due to the radiative cooling caused by the fog layer, SST became much warmer than the air temperature.

The LL wind direction appears to be a significant factor in fog formation along the trajectory at the point O (Figure 19d). The winds for the first part of the period were consistently from the west throughout the entire layer. The TKE is weak near the surface and likely generated by the wind shear and not buoyancy due to the negative heat flux. However, about an hour prior to the fog formation the winds abruptly shifted from westerly to southerly from the surface up to 100 m above. This wind shear generated turbulence not within the fog layer, but above fog layer where the stable stratification was weaker and the wind shear was moderate. In spite of the radiative cooling at the top of the fog layer, it did not experience turbulence because of the strong stratification which inhibited TKE from developing. As for the shifting in winds prior to the fog formation, it appeared that a mesoscale fog-induced pressure gradient force was generated between the cold, dense fog layer and the less dense air to the west. As the air began to encounter the higher pressure (fog layer) the flow was diverted parallel to the fog region in driving the flow in a northward direction (Dalu and Baldi 2003). This mesoscale boundary was consistent throughout the model simulation and is a possible reason for the 90° shift in the winds ahead of the fog layer.

Through the evolution of the trajectory, the dominant westerly wind and the surplus of water vapor in the area, along with high static stability and cooling MABL, were the contributing factors in the initial formation of the fog over the YS.

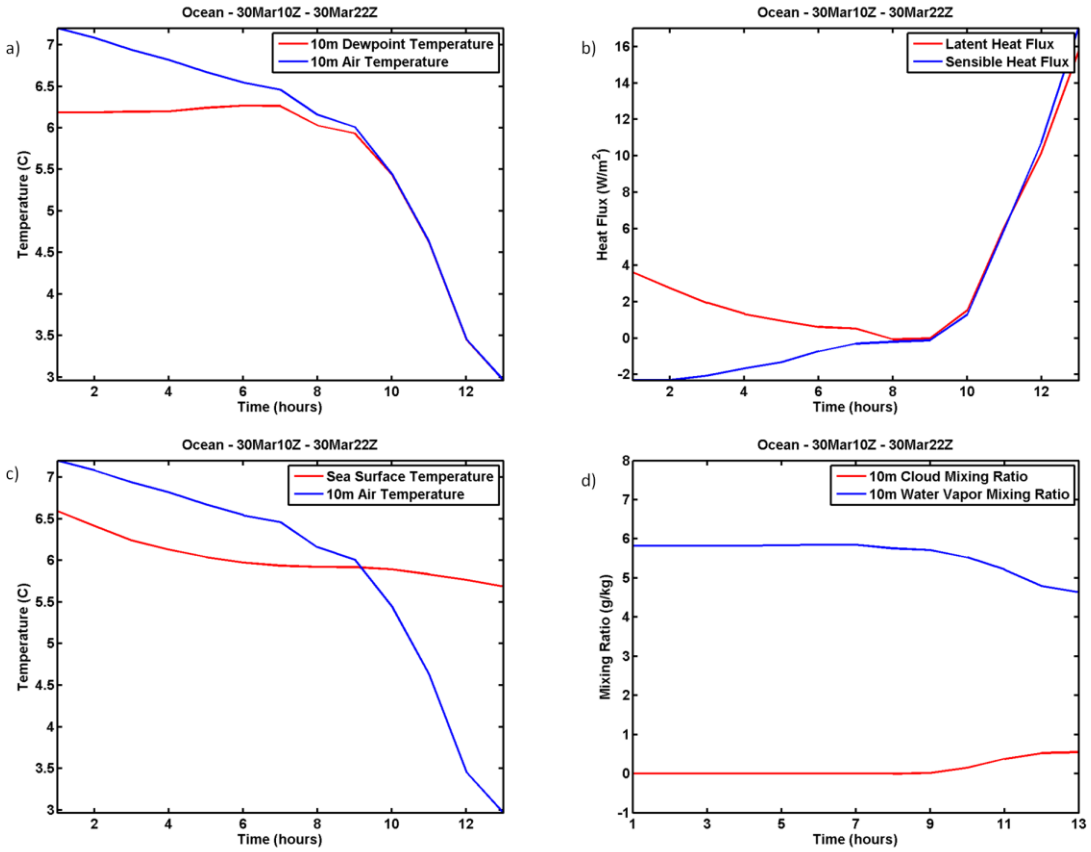

Figure 20. Surface variables along the point O trajectory from 30 March/10Z to 30 March/22Z. a) 10 m dew-point temperature and 10 m air temperature; b) LHF and SHF; c) SST and 10 m air temperature; d) 10 m q_c and q_v.

2. Kunsan

The forward trajectory of the air prior to the formation of fog over Kunsan AB represents both ocean and land characteristics due to its proximity to the coast. Figure 21 shows the 12-hour trajectory of the air that originated over the ocean and flowed west-northwesterly until it reached the base. It is important to note that the air parcel became virtually stationary immediately prior to fog formation. This indicates that the fog region in a stable environment was also experiencing minimal surface winds, which is different from the point O trajectory which depicted a southerly flow prior to the fog. This suggests that the aforementioned mesoscale pressure gradient, was not established for a long enough period of time to result in a modification of the flow at Kunsan AB.

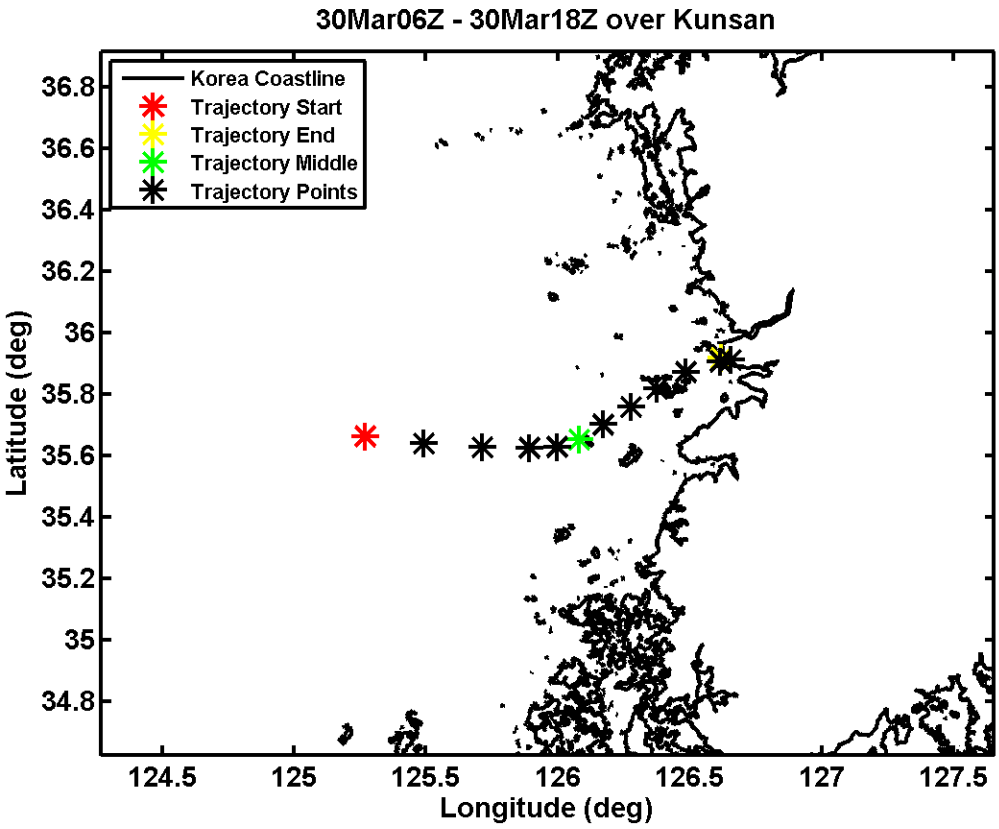

Figure 21. Kunsan AB - The forward trajectory path of the air beginning to the west (red star) and ending at the point of interest when the fog began (yellow star).

Similar to the fog formation over point O, the q_v shows an increase prior to the formation with a decrease during the fog (Figure 22c). Also, the q_c (Figure 22a) shows an increase around hour 10 of the trajectory that represents the fog layer. An interesting difference between this trajectory and the ocean one is the depth of the fog layer. The pervious fog layer was only at most 100 m deep, while coastal based fog layer was twice as high up to 200 m. This factor was due to a less stable environment over the land and the fact that this fog originally formed as a land based radiation fog. The formation time occurred over night when the cooling was maximized and the increase in moisture made the environment susceptible for saturation.

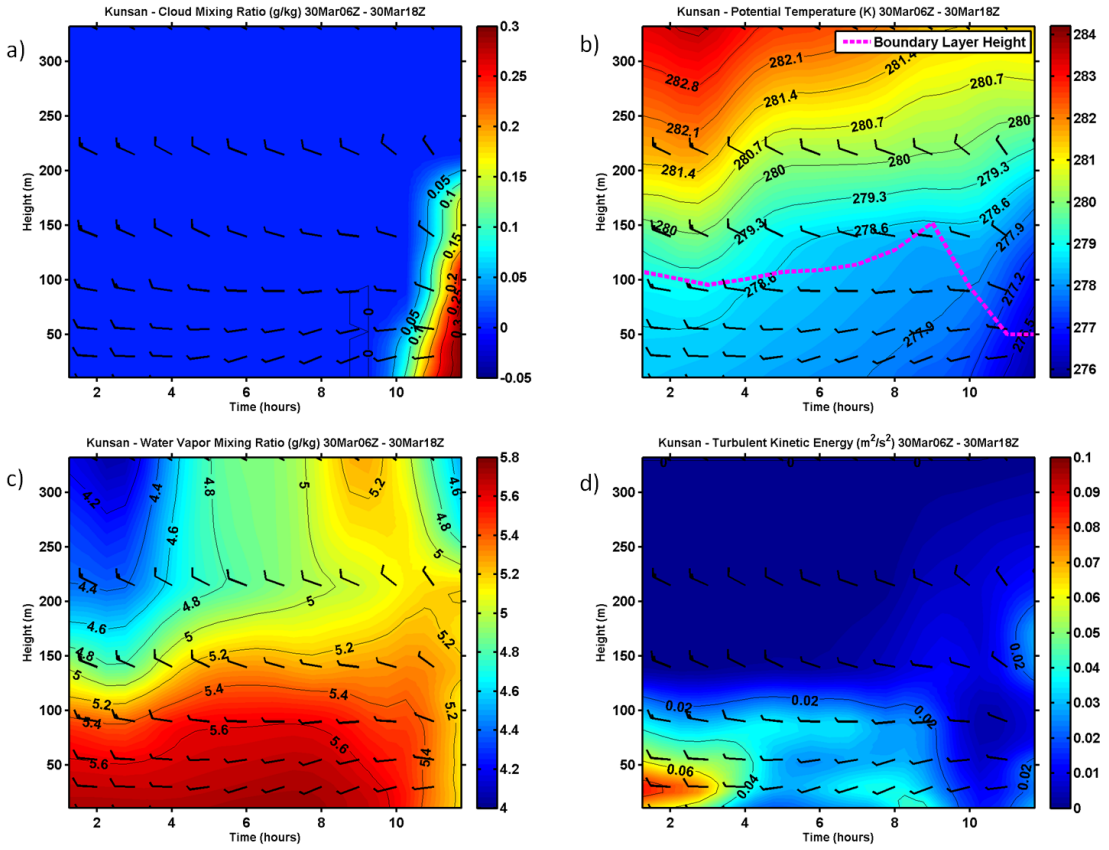

Figure 22. Contour plots along the Kunsan AB trajectory from 30 March/06Z to 30 March/18Z. a) q_c; b) potential temperature with BL height; c) q_v; d) TKE. Wind barbs represent the wind speed and direction of the flow in knots. The height level is up to 330m.

The potential temperature profile (Figure 22b) leading up to the fog formation was weakly stratified in the evening and well mixing during the day. The stratification increased over the time of the trajectory, similar to the point O trajectory. The evolution of the surface based variables along the Kunsan trajectory (Figure 23) has some similarities, but some differences compared to the point O trajectory. A unique feature in these plots is the steady drop in air temperature along the path as the heat from the air was lost over time since the SST was around 1°C less than the air temperature. This heat loss continued until the air parcel formed fog and the air temperature dropped 2–3°C in the fog.

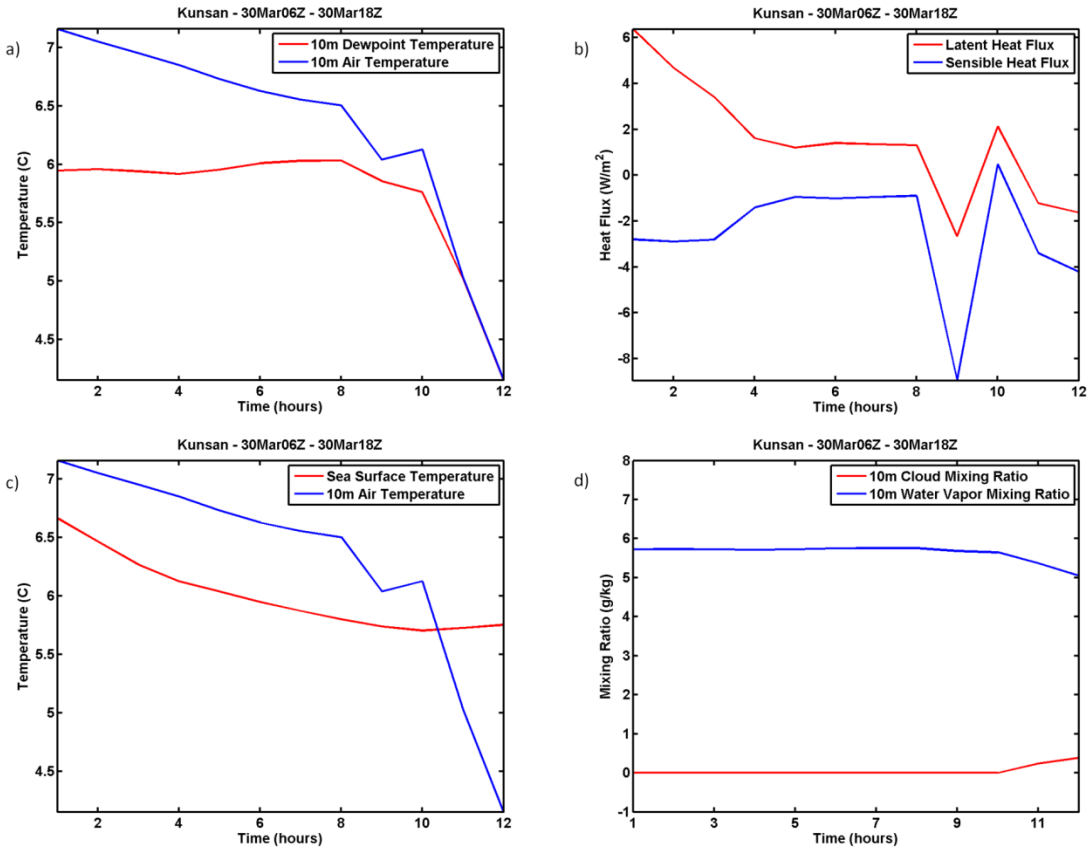

Figure 23. Surface variables along the Kunsan trajectory from 30 March/06Z to 30 March/18Z. a) 10 m dew-point temperature and 10 m air temperature; b) LHF and SHF; c) SST and 10 m air temperature; d) 10 m q_c and q_v.

Also, another resemblance between the two paths was that the dew-point temperature (Figure 23a) increased throughout the path until the air temperature dropped to reach the dew-point temperature leading to saturation. All of these characteristics are consistent between the trajectory paths. However, the major difference were considered when analyzing the LHF and SHF between the two paths.

With regard to the LHF and SHF shown in Figure 23b, it was apparent that the differences in the fluxes between the two trajectory were driven primarily by the surface feature, *i.e.*, land vs. water. In the beginning portion of each trajectory, the SHF and LHF were consistent, because each path originated over the ocean surface. However, once the air parcel encountered the land the fluxes change significantly. For instance, at hour 8 in

the Kunsan trajectory both the LHF and SHF became negative. This occurred only when the trajectory passed over an island off the coast of Korea. This island contributed to the negative fluxes because of the lower temperature and less moist surface on the island at night compared to the ocean surface. When the parcel continued to progress westward it began to encounter the water again, which increased the fluxes until fog formed at hour 10 and the LHF and SHF became negative. Unlike the point O trajectory, when the parcel was in the fog, the fluxes decreased immediately after the fog formed.

This coastal based trajectory has similar characteristics to the air over the ocean, but also is driven by the difference in the land features that also play a role in the formation and evolution of the fog formation.

2. Inland Location

Figure 24 represents the flow of the air 10 hours prior to fog formation over point L. This trajectory showed very similar quality compared to the previous two trajectories. This air path started over the water and progressed eastward until it reached the land when the parcel slowed down and turned more southerly 1 to 2 hours prior to the fog forming. This trajectory was also carried over less of the water than the other two paths. Therefore, the land influences tended to dominate the characteristics of the formation process responsible for fog formation. This type of fog may not be classified as a sea fog, but due to its close proximity to the coastline the formation is aided by characteristics of the air parcel's origin and follows the advection-radiation fog description in Gultepe *et al.* (2007).

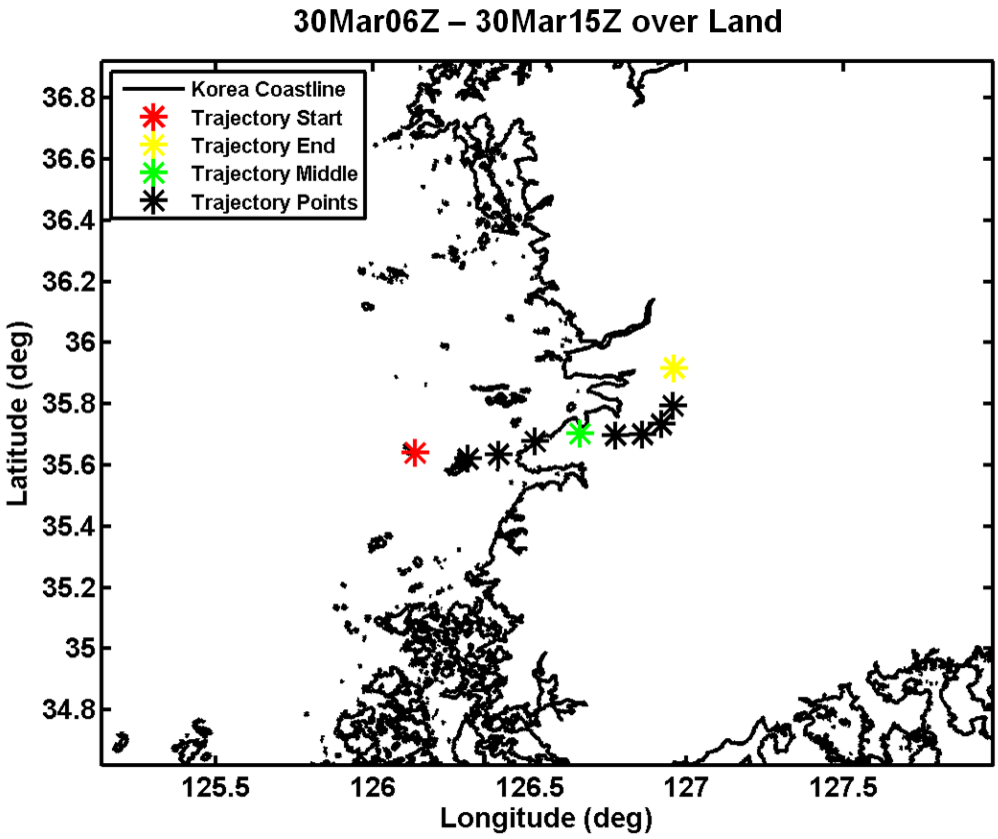

Figure 24. Point L - The forward trajectory path of the air beginning to the west (red star) and ending at the point of interest when the fog began (yellow star).

The q_c plot shows a very shallow fog layer over point L in Figure 25a similar to point O's fog formation period. Also, the q_v plot shows an abundance of water vapor throughout trajectory leading up the fog. These patterns were very consistent with the previous mixing ratio plots. However, when examining the potential temperature plot (Figure 25b) it was evident that the stable stratification varies throughout the path. There seemed to be more variation in the thermal structure in the BL during this period. There was more representation of diurnal effects over the land compared to the previous figures. Also, when the air column reached the land, the daytime heating increased the temperature and created a more well mixed BL. This fact can also be seen on the TKE plot (Figure 25d) where the increase in the BL was seen when the parcel was over the land, but the TKE began to decrease as the thermal structure became stably stratified

which inhibits turbulence mixing within the BL. The wind also resembled those from Point O and Kunsan with steady westerly flow and increase in moisture throughout the time period of the trajectory. These conditions led to a favorable environment for fog formation.

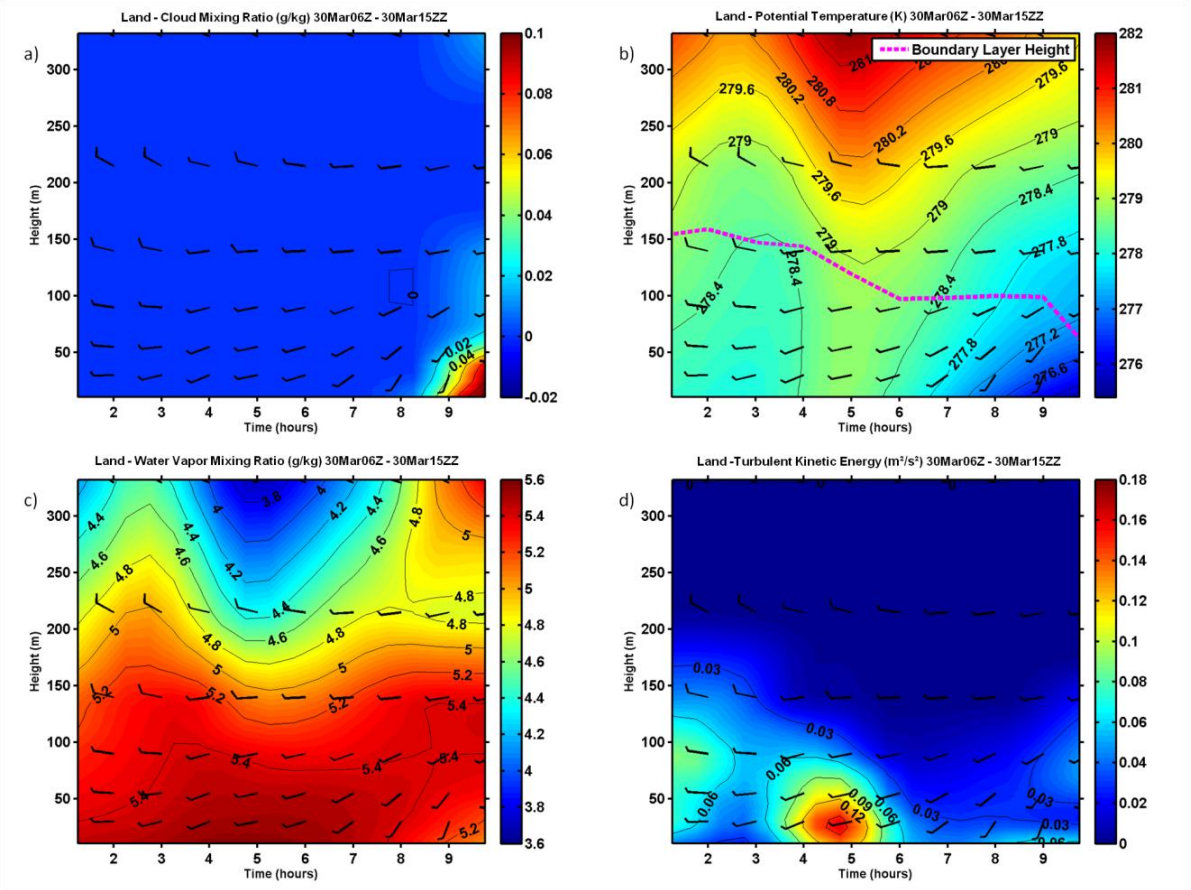

Figure 25. Contour plots along point L trajectory from 30 March/06Z to 30 March/15Z. a) q_c; b) potential temperature with BL height; c) q_v; d) TKE. Wind barbs represent the wind speed and direction of the flow in knots. The height level is up to 330m.

The three panels, in Figure 26, for the surface features are analyzed along the trajectory arriving at point L trajectory in comparison with those from Point O and Kunsan. Note that the SST and air temperature difference is not shown in this figure as for the other two points of interests because of the relative short time the air column experienced over the water. After looking at two similar trajectories, it became apparent

that the structure of the 10 m air and dew-point temperatures were consistent. However, for the point L trajectory, there were some subtle differences. For instance, the air temperature began to drop much before the fog formation (3–4 hours). This is likely due to the effects of the diurnal evolution over the land, where the land temperature dropped much more rapidly after sunset than it did over the sea. Then once the temperature dropped 2°C, the air became saturated and fog formed. Also, the dew-point temperature was 1 to 0.5 °C less than that along the Kunsan trajectory, which was likely due to Kunsan's closer proximity to the moisture source.

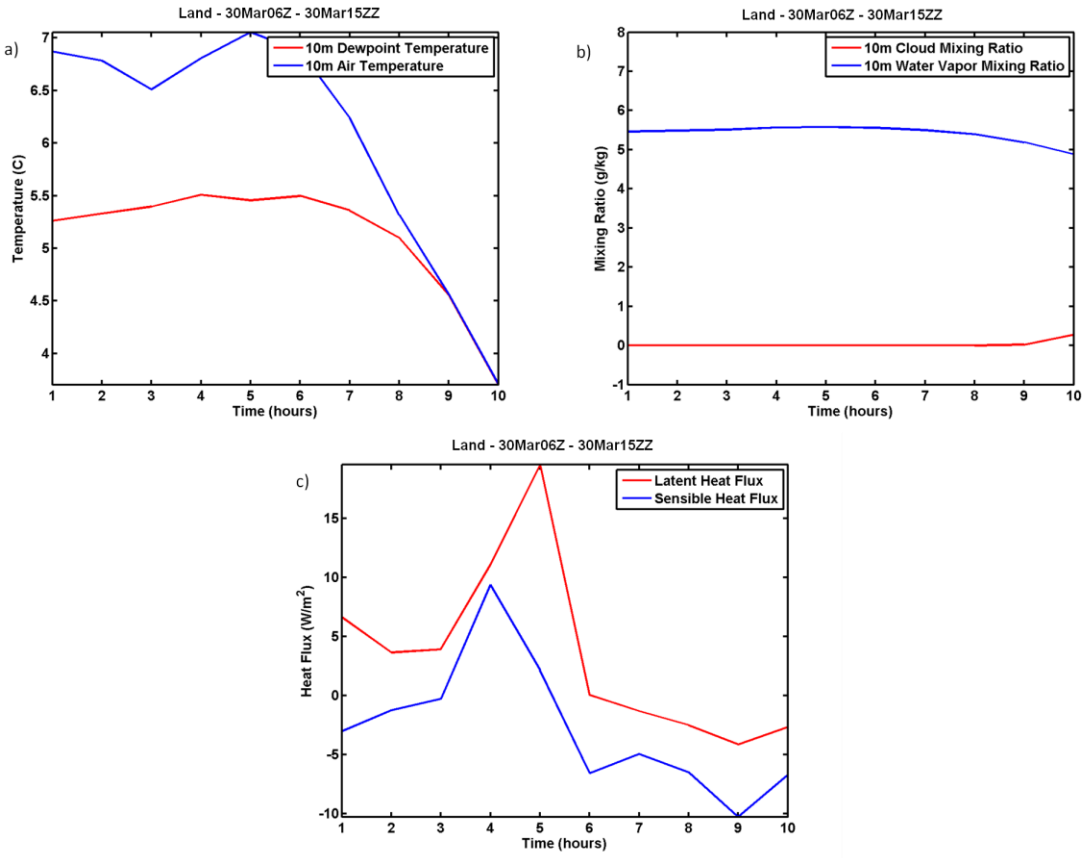

Figure 26. Surface variables along the Kunsan trajectory from 30 March/06Z to 30 March/15Z. a) 10 m dew-point temperature and 10 m air temperature; b) LHF and SHF; c) 10 m q_c and q_v. Comparison of the air temperature vs. SST was omitted since parcel was primarily over the land.

The LHF and SHF plot (Figure 26c) is also different than those from the previous two trajectories. Over the first few hours of the trajectory the SHF was negative because SST was lower than the air temperature. However, once the air reached land both variables start to increase sharply in concert with the increase in land temperature. Then once the temperature began to drop during hour 5, so did the fluxes, until they dropped below zero and stayed there through the early part of the radiation fog. The negative SHF and LHF were due to the fact that the surface layer was stable and the air was saturated after the fog was formed. These variations in the SHF and LHF over the land vs. the water are critical factors to consider when examining whether or not to forecast fog, either sea or radiation fog based.

In conclusion, the three trajectories which were analyzed either over the ocean, over the land, or over both represent different aspects of the formation of fog. A major difference was the contrast in the surface characteristics between the land and sea. These differences drove the considerable variability in the SHF and LHF, which leads to variations in the fog evolution for different locations. However, some key factors that were consistent over all the trajectories were the increase in moisture over time and distance and the decrease in temperature prior to fog formation.

C. EVOLUTION OF FOG FORMATION AND MAINTENANCE AT SPECIFIC LOCATIONS

This section examines the variations of the BL and surface features at each point (point O, Kunsan, and point L) to examine the dominant physical processes during the life cycle of fog. All of the time series analyses cover the entire period (72 hours) during which fog was simulated at the respective locations. Similar to the previous analyses, an examination of the near surface conditions and the vertical variations were conducted to gain a better understanding of the air-sea interaction that is important to the sustainment of the fog. The following variables were plotted: q_c, potential temperature, SST and 10 m air temperature comparison (for point O and Kunsan only), and surface LHF and SHF.

1. Coastal Ocean Location

The q_c plot (Figure 27a) over point O shows fog forming around hour 18 and lasting through hour 60. This fog underwent various modifications throughout its lifecycle. Initially the fog liquid water content, q_c, was relatively low, extending as high as 100 m. However, as the fog persisted over point O the BL height (Figure 27b) dropped from near 100 m to 50 m. The fog layer remained near 50 m for approximately 1.5 days and was most likely sustained through fog layer top longwave radiative cooling and steady subsidence synoptic conditions, which helped to maintain the strong LL inversion. Also, the winds prior to the fog were westerly with a weak southerly component. The BL depth increased and the q_c decreased after a strong, drier northerly wind approached the region. The fog layer dissipated after hour 60 in the northerly wind condition. The potential temperature profile early in the period displays a well mixed BL until the fog formed with LL stratification increasing throughout the period of the fog. The BL became well-mixed following the dissipation of the fog layer.

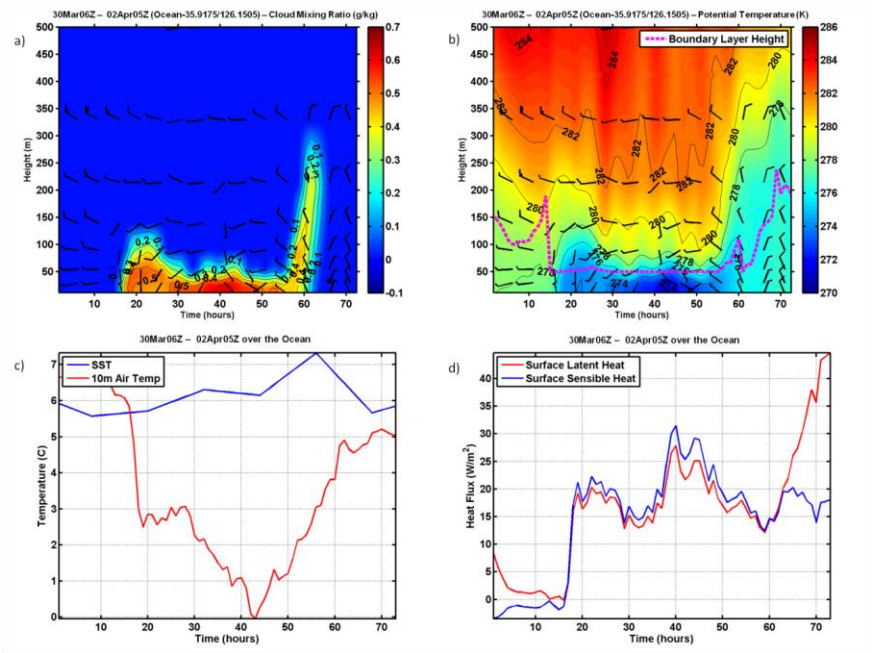

Figure 27. The contour plots and surface plot time series analysis from 30 March/06Z - 02 April/05Z over point O in the YS due west of Kunsan AB. a) q_c; b) potential temperature with BL height; c) SST/10 m air temperature; d) surface LHF/SHF.

Further examining the SST and the 10 m air temperature (Figure 27c) reveals that fog formed, when the air temperature dropped below the SST. The air temperature decreased substantially in the fog layer where air temperature was about 6°C below the SST at the peak of the fog. As the fog liquid water amount decreased, the air temperature began to rise until the fog dissipated. As for the LHF vs. SHF (Figure 27d), their characteristic resembled those of the point O trajectory mentioned in the previous section. The LHF was positive and decreased towards zero while the SHF was negative and increased towards zero. This occurs because the air is not saturated, and because the air temperature was warmer than the SST and decreased with time. Once the fog formed an abrupt increase in LHF and SHF occurred due to the significant radiative cooling and the air becoming saturated. The parallel variation in the fluxes continued and varied slightly throughout the life time of the fog. The slight variations in the fluxes were driven by the changes in the density and depth of the fog layer with time. When there was heavily dense fog, the fluxes increased, while the opposite caused a decrease in the fluxes. As the fog dissipated, the LHF went even more positive due to the drying of the air relative to the sea and the SHF remained primarily constant due to the fact that the SST remained warmer than the air as cooler, drier air advected in from the north.

2. Kunsan Location

The Kunsan time series analysis displays characteristics of both the marine and land environment. This is clearly shown in the q_c plot (Figure 28a) compared to that at Point O (Figure 27a), where the diurnal variations over the land led to fog burn off during the daytime. The initial patch of fog during hours 12 to 24 has been characterized as being land based fog that developed over night in the presence of an increase in LL moisture and a decrease in air temperature. However, the second patch of fog can be considered a sea based fog, since it occupied an area of the sea just off the coast of the base. Prior to the formation of the second fog area, a period of westerly winds (sea breeze) dominated the BL causing conditions favorable for fog. The winds above the BL were also light and variable throughout the second period of fog, which was different than the initial fog period. When the northerly winds increased to 15 kts and brought in

drier air, the fog disappeared as the cloud water were lifted above the surface. The potential temperature contour plot (Figure 28b) over the coastal region shows a stable stratification and shallow MABL throughout much of the LL even during the day when no fog was present. Only a small increase in the MABL height during the day suggests the strong influences from the cooler sea environment preventing significant warming and turbulent mixing as will be described at land point (Point L) later.

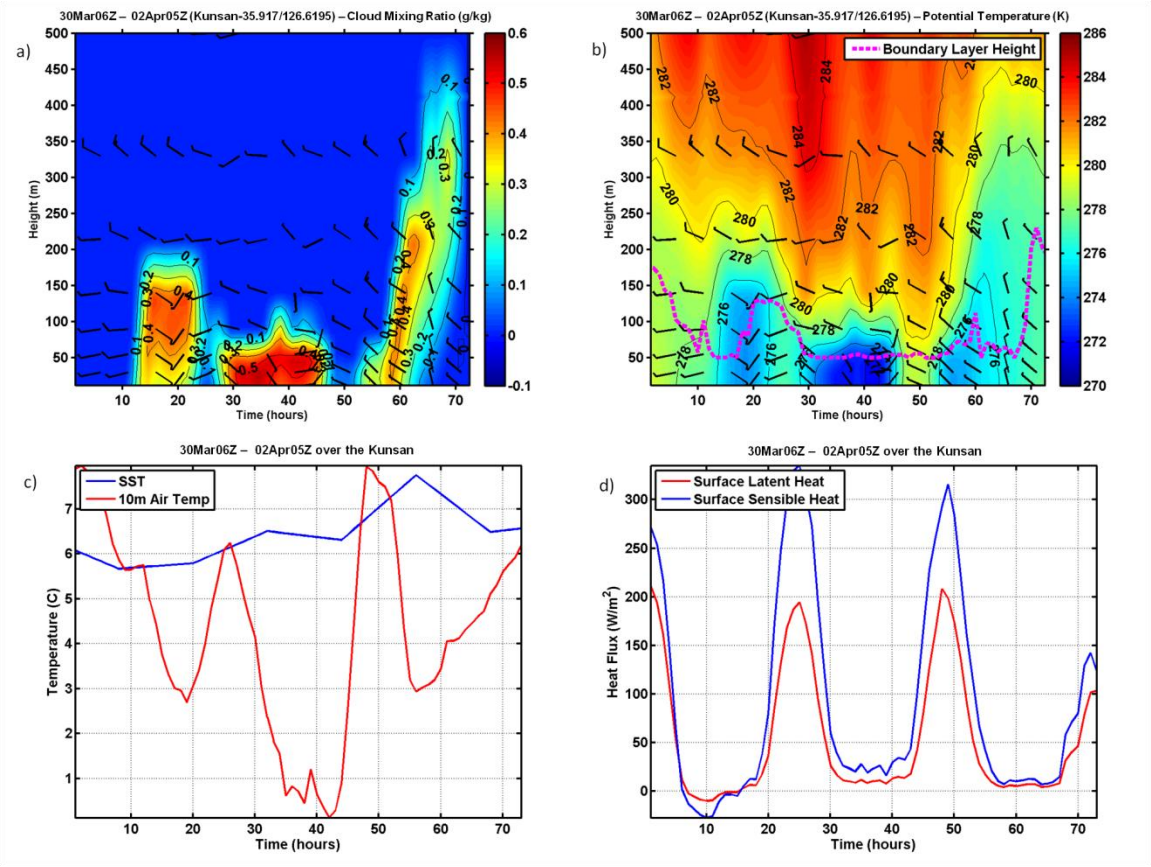

Figure 28. The contour plots and surface plot time series analysis from 30 March/06Z - 02 April/05Z over Kunsan AB along the west coast of the Korean Peninsula. a) q_c; b) potential temperature with BL height; c) SST/10 m air temperature; d) surface LHF/SHF.

The SST and 10 m air temperature plot (Figure 28c) shows the diurnal changes between day and night. This diurnal variation had a profound influence on the fog layer as the fog dissipated with daytime warming. The LHF and SHF (Figure 28d)

experienced significant diurnal variation, which were also similar to the land point with smaller magnitude. Since Kunsan AB is situated at the coast, it was apparently affected by both land and ocean environments. As a result, when the more dense region of fog dominated the area on the second day, small but positive fluxes occurred. These positive fluxes were a result from the surface being warmer than the near surface air. The surface cooling was also minimized due to the fog cover.

3. Inland Location

The q_c plot (Figure 29a) associated with point L shows similarities to the Kunsan and point O with less time in the fog. Each of the periods of fog experienced by the land base points occurred during the night hours when the temperatures were low enough due to radiative cooling to support fog. The winds prior to each fog period reflect an onshore or westerly flow that was likely associated with the local sea breeze circulation. This circulation drove in the marine environment and likely led to the advection of the sea fog. Within the first two fog periods the winds began southerly, but turn to easterly due to land breeze established at night. During the third fog period, the winds were primarily out of the northwest associated with the frontal boundary from the north. The potential temperature and BL height plot (Figure 29b) show a much more drastic fluctuation in thermal structure throughout the period. The BL height within each of the fog periods were lowered to 50 m as seen in the previous BL plots. However, during the day the LL turbulence due to surface heating drove the BL up to above 400 m (convective mixed layer). As the temperature dropped prior to the fog formation, the stable stratification regenerated making it favorable for fog.

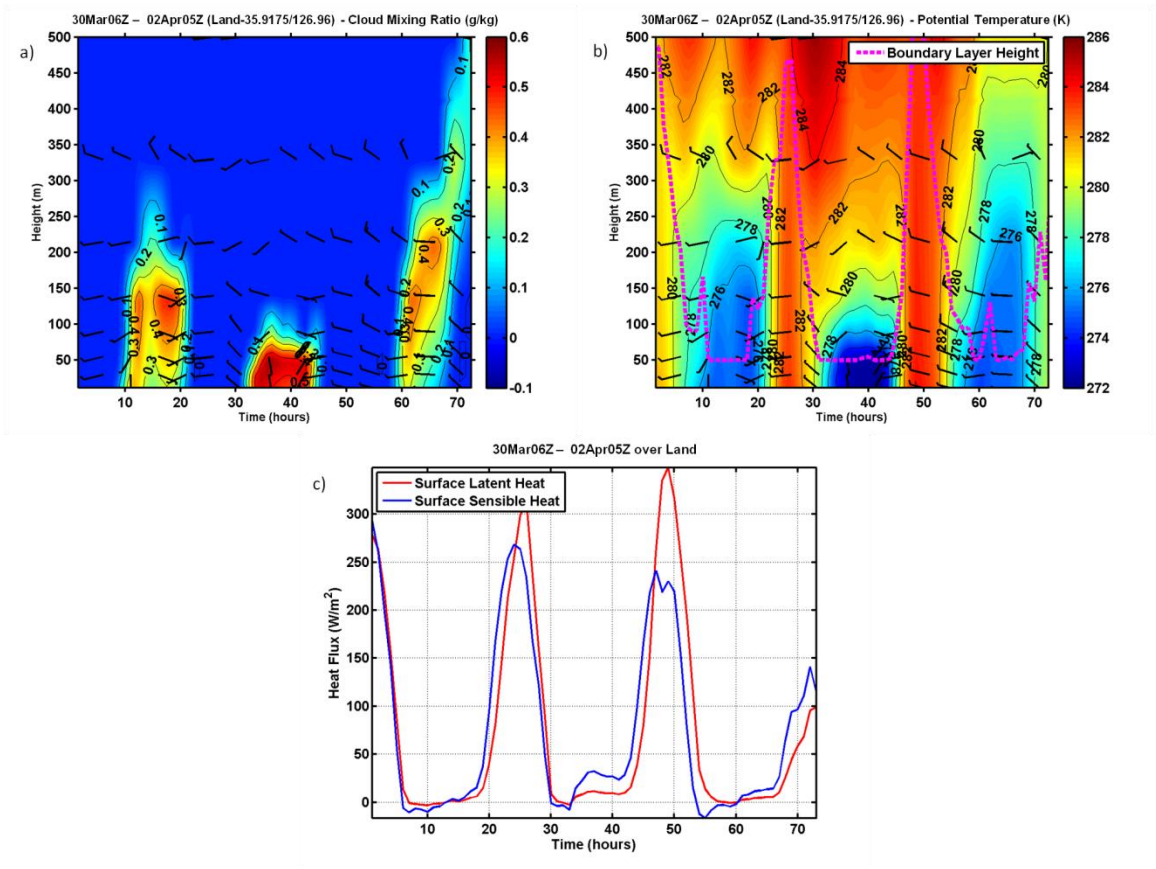

Figure 29. The contour plot and surface plot time series analysis from 30 March/06Z - 02 April/05Z over point L on the Korean Peninsula due east of Kunsan AB. a) q_c; b) potential temperature with BL height; c) surface LHF/SHF.

Since point L does not encompass the YS, a SST vs. 10 m air temperature plot was omitted. Therefore, when analyzing the surface variations at point L, only a LHF/SHF (Figure 29c) plot was constructed. Similar to Kunsan, the LHF/SHF shows the diurnal variations very clearly. As the land heated up during the day, both the LHF and the SHF increased considerably.

Examining the time series at the three different points showed the variations of the fog through the life cycle of the event. Point O experienced continuous; Kunsan and point L showed diurnal variations of the fog indicating that the fog was driven by the surface fluxes and thermal structure near the surface. The synoptic scale feature that influenced the consistency of the environment was a major factor in the overall

dissipation of the fog. When the cooler and drier air pushed in from the north all of the LL clouds lifted off the surface and were eventually dissipated. This time series analysis gave us a clearer understanding of the effects associated with the different surface features and the evolution of the fog over time. The next section will examine a different aspect of the fog through a vertical cross section analysis.

D. SPATIAL VARIABILITY IN STAGES OF FOG DEVELOPMENT

To investigate the spatial variability in the coastal region of Kunsan AB, a straight path from the central YS to central ROK (Figure 30) was constructed. In addition, vertical variations of boundary layer thermodynamic and surface properties were examined, which helped to explain the surface fluxes and LL static stability that occurred during the life cycle of the fog event. The variability along this vertical cross-section was critical in determining the structure of the environment that led to the onset of fog and the eventual dissipation that occurred at the end of the simulation. The following sections will discuss the results from these vertical cross-section analyses to help understand the mechanism and air-sea modifications that contribute to advective sea fog as simulated in this case.

In this analysis, the cross-sections extend a horizontal distance of over 250 km from 125°E to 128°E. From this vantage point, it was possible to depict the fog throughout the region and to see the variations of the fog at each of the three points of interest described in the previous sections. From the 72-hour model run, the following variables were analyzed: 1) BL q_c; 2) BL potential temperature; 3) surface LHF/SHF; and 4) SST and 10 m air temperature. These variables were examined during three different times at the beginning, middle, and the end of the fog period, respectively. This will show the characteristic of the environment at the critical stages of the fog development to include the formation, maintenance, and dissipation stages.

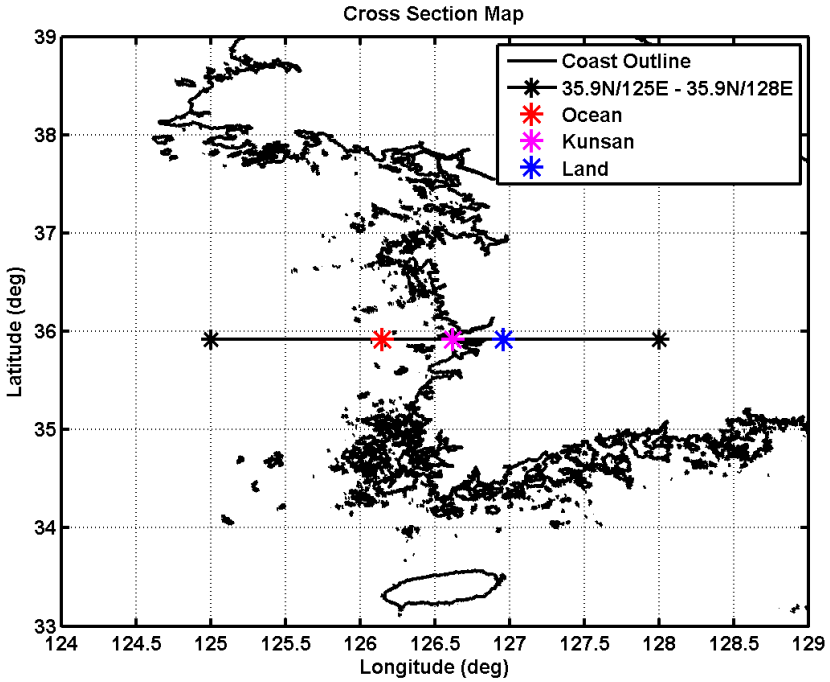

Figure 30. Map of areas used for cross section

1. Initial Fog Formation

Figure 31 shows the variables during the middle of the night when the initial fog period occurred over the land on 30 March/18Z. The q_c plot (Figure 31a) shows the initial fog period extending above 330 m even though the BL height as indicated on the potential temperature plot (Figure 31b) was near 50 m. The potential temperature profile shows a moderately stable BL setting up over the land with a weakly stable layer over the ocean. The winds over the ocean at 18Z were from the west continuously advecting moisture over land. About 50 km ahead of the fog region, the winds near the surface show a weak southerly component up to 100 m. This suggests that the fog boundary was creating a pressure gradient which modified the wind flow west of the fog. Wind within the fog layer switched to easterly off the land. The easterly winds were created by the differential thermal structure between the cooler fog layer and the relatively warm marine environment. The thermal circulation resembled a land/sea breeze circulation and caused the fog layer to advect off the land surface and over the water. Therefore, as the daytime

heating began to burn off the land fog, the fog event transferred from a land based fog to a sea based fog. Since the sea surface conditions were suitable for the fog sustainment, the fog became sea fog.

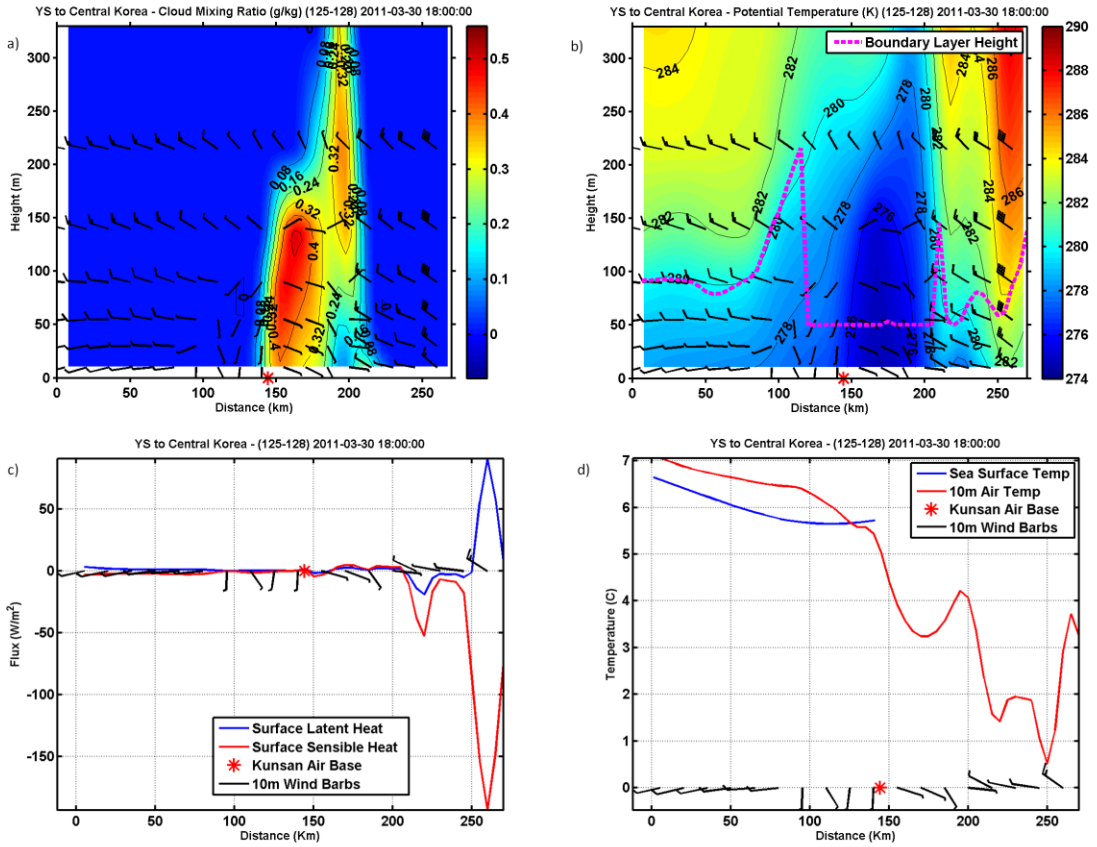

Figure 31. The four plots represent the vertical cross section (a and b) and near surface properties (c and d) along the line described in Figure 16 at 30 March/18Z. a) cloud water, q_c; b) potential temperature; c) surface LHF/SHF; d) SST/10 m air temperature. Wind barbs on (c and d) represent 10 m wind speed and direction. The red star at 147 km shows the land/sea boundary along the cross section with land surface to the right. SST in d) is only up to the land-sea boundary.

Variation of the surface LHF and SHF (Figure 31c) were dominated by the extremely large magnitude of negative sensible heat flux well into the land surface. It is not likely that such large negative heat flux is realistic. As shown in all previous discussions, LHF and SHF are both small (<10 $W \cdot m^{-2}$) over much of the sea. The LHF

over the ocean was slightly positive, but the SHF was slightly negative due to the stable stratification. These conditions tended to increase LL moisture and reduce LL temperature and hence generated a favorable environment for the fog to form over the sea.

In addition, the decreasing air temperature (Figure 31d) and the light winds within the fog layer help maintain the fog layer. Also, the decreased air temperature near the coast region enabled the fog to survive over the water after the shortwave radiation heated up the land during the early morning hours and through the day on 31 March.

2. Sustained Sea Fog

The plots in Figure 32 shows the environment along the cross section during the late afternoon hours on 31 March/09Z. It is clear that the fog region represented by the q_c color contours (Figure 32a) have changed not only in location but also in volume compared to the initial period the previous night. In this figure, the layer of fog decreased in depth to only 50 m, which corresponds well with the COAMPS diagnosed BL height (Figure 32b). This decrease in depth had to do with the increase in the near surface stability and subsidence associated with the large scale synoptic forcing. The fog bank was hugging the coast line near the red star, which indicates the location of Kunsan AB. However, the higher cloud water of 0.5 $g \cdot kg^{-1}$ was over the sea where the conditions were optimal for sea fog development.

The fact that Kunsan is directly on the coast is one of the major reasons of the difficulty in this forecasting challenge. One of the major factors that determines whether or not the fog will impact the base is the LL winds. In this case, the winds within the fog were primarily from the south, however, on the eastern edge of the fog bank the winds were westerly, which was a reason for the fog advecting inland slightly. This advection of fog was again driven by the differential heating between the land and the sea and the thermal circulation that ensued. Therefore, there appears to be a balance of forcing occurring between the heating of the land, which dissipates the fog and the advection of conditions favorable for fog onto the coast. The balance of the two mechanisms (shortwave radiation and thermally driven circulation) is the driving force behind the

inland propagation of the fog during the day. Potential temperature (Figure 32b) shows the fog layer to experience significant stable stratification. While the nearby land surface encountered a decrease in stability generating turbulence in the LL and an increase in the BL height. The southerly component of the wind over the sea was contributing to the horizontal flux of moisture and heat which was continuing to support the fog over the sea.

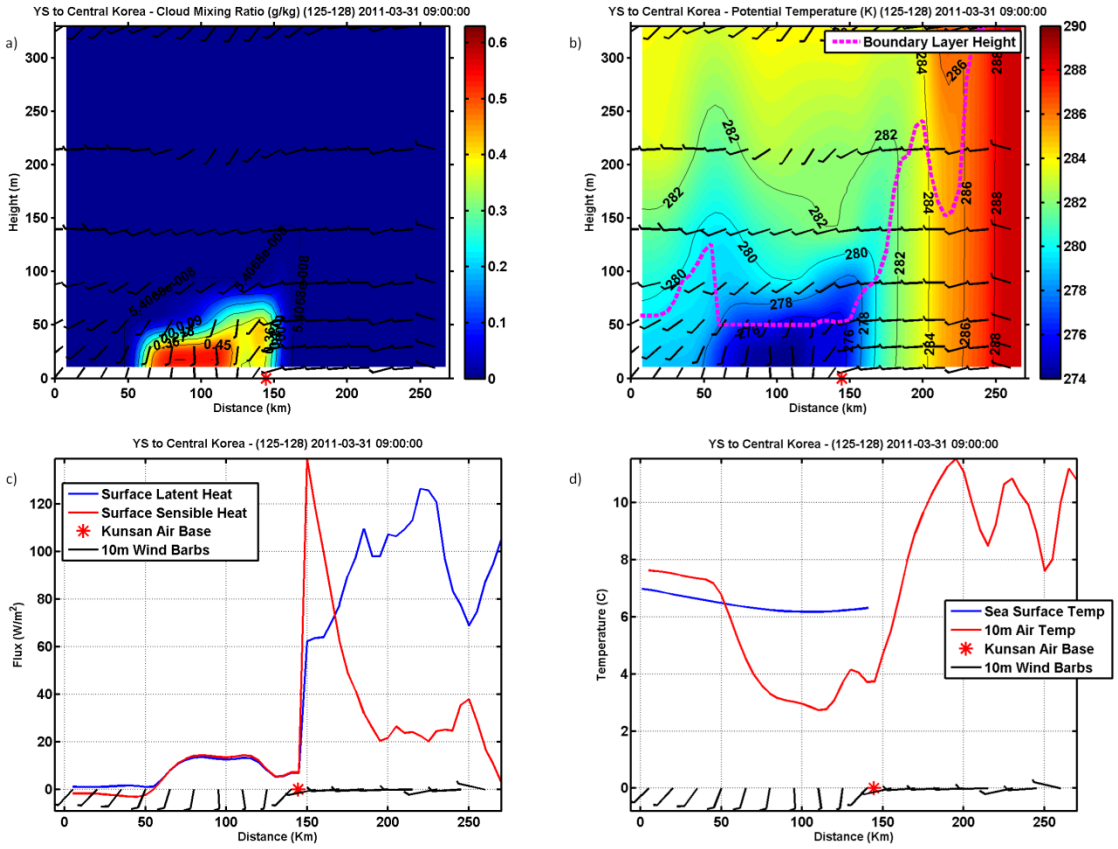

Figure 32. Same as in Figure 31, except at 31 March/09Z.

The near surface properties at this time also differed from those in Figure 31. Now that the shortwave radiation was the dominant heating source, the surface fluxes over the land were all positive, while the fluxes over the sea still were relatively low. The fluxes show a significant jump once the land surface heating effects came into play. This increase in the heat fluxes over the land made it difficult for the fog to form. As for the SST/10 m air temperature comparison, there was an obvious decrease in temperature

within fog with a sharp increase in temperature over the land. Also, the air temperature to the west of the fog (left of 50 km) over the ocean was larger than the SST in the region and was the reason why the fog has not formed there yet. Once the contact cooling took effect in that region the air temperature decreased to the dew-point temperature causing saturation to occur and fog to form. Now that the sea fog is well developed and the synoptic pattern was such that the sustainment of the fog was highly probable, let's consider the time period when the sea fog advected back onto the land.

At this point in the simulation, the fog has moved from the land to the sea and has moved back on to the land, however, the depth of the fog has remained shallow displaying similar characteristics as when it was over the sea. Between the Figure 32 and 33, the fog has increased in size and density as evident from the increase in the q_c values (Figure 33a). Also, during this time the sun set enabling the land temperatures to drop and the fog to form over the land. In addition, the winds went from west-southwesterly in Figure 32 to east-southeasterly in Figure 33. This land-sea breeze circulation that occurred allowed for the migration of the fog from land to sea to land over a 24 hour period.

The potential temperature shows a clear boundary between the cooler fog layer and the relatively warmer land. Comparing the BL height from Figure 31b to Figure 33b, there's a clear indication that the BL height was uniform across the cross section, creating an BL suitable for fog formation by trapping the fog below 50 m.

The LHF/SHF plot (Figure 33c) is similar to the plot in Figure 31c over the land near 250 m, suggesting that the conditions farther inland were not affected by the MABL. However, over the coastal and YS region the LHF/SHF was indicative of positive surface fluxes suggesting a fog layer as described in Section 4.C.1. The boundary between the fog and no fog occurred when the SHF dropped below negative and the LHF leveled off and slowly began to increase. As for the SST/10 m air temperature there was a definitive demarcation between fog and non-fog areas. The region where the air temperature was below the SST was where the fog layer occurred. But when looking on the land, as the air temperature began to increase between 150 and 200 km the fog began to dissipate. Once the air temperature began to increase to a peak, there was a clear boundary between

fog and no fog. As the shortwave radiation began the next day, the sea fog which advected inland retreated back to the sea and remained over the YS. The next analysis will examine the mechanisms which led to the demise of the sea fog and eventually caused the event to finish by the end of 01 April 2011.

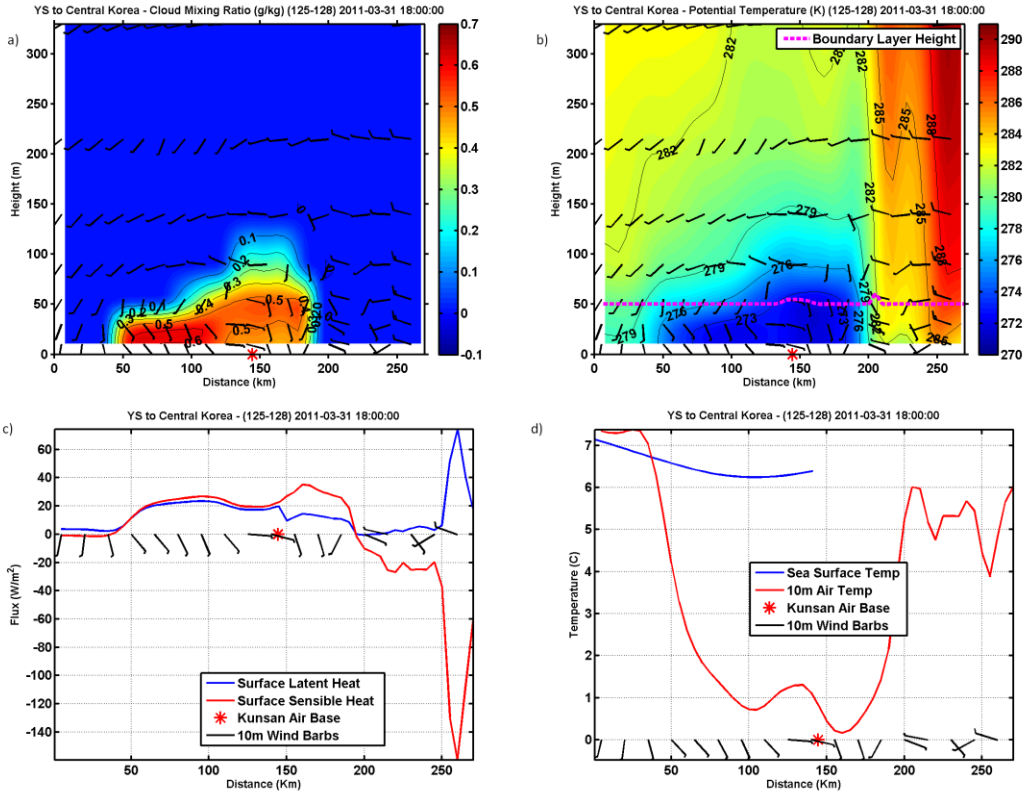

Figure 33. Same as in Figure 31, except for 31 March/18Z.

3. Sea Fog Dissipation

The dissipation of the fog event occurred as a result of a synoptic pattern change due to an approaching frontal system from eastern China. This pattern changed the LL environment, resulting in an increase in the BL height and a decrease in q_c and eventually led to fog dissipation.

Figure 34 represents the early stage of the dissipation period and shows some key features associated with the ultimate end of the fog in the simulated event. The q_c plot (Figure 34a) shows the elevated fog layer on 01 Apr/18Z. The lifting of the fog occurred

during the increase in the northerly winds which were increasing on the west size of the cross-section from 5 to 20 kts. With the increase in the winds, the BL height (Figure 34b) increased from 50 m to nearly 250 m over the ocean. In addition, the potential temperature profile was also indicting a well mixed LL to the west of the fog and a decrease in stability throughout the cloud layer. The low temperature associated with the fog were advected inland with the fog layer as the near surface winds continued to resemble the thermal circulation that was driven by the differential heating between the fog layer and the land.

With the stronger northerly wind to the west of the fog, the LHF/SHF (Figure 34c) show an increase in LHF in that region. This increase in LHF is likely due to the advection of drier air associated with the approaching frontal system. However, the increased water vapor from surface evaporation is not strong enough to balance the drying from advection by the northerly wind and eventually led to an environment not conducive for fog formation.

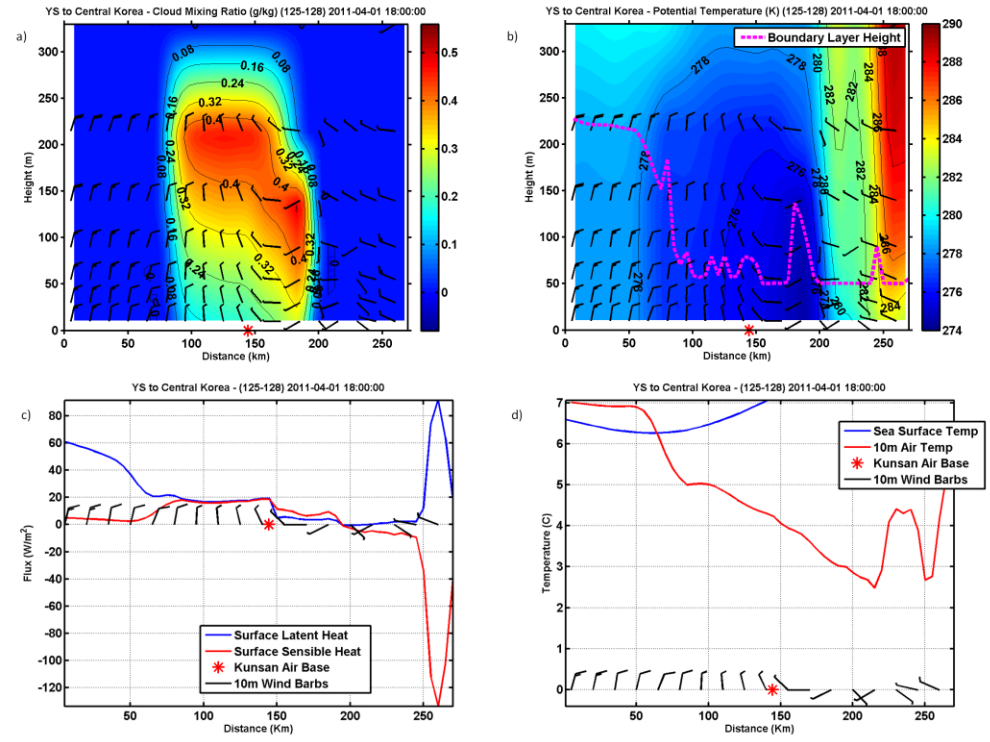

Figure 34. Same as in Figure 31, except for 01 April/18Z

In summary, the lifecycle of the fog from the initial formation over the land to the transition to sea fog to the ultimate dissipation underwent many variations. These changes in the LL environment and thermodynamic properties were well identified and noted in this section. It became apparent in this simulation that the fog was controlled by the thermal structure over both the land and sea and the subsequent circulation driving the fog from land to sea and back to land. As long as the subsidence and longwave radiative cooling persisted, the fog appeared to expand as the air on the leading edges continued to cool to the point of saturation. As the synoptic pattern changed and cooler, drier air pushed into the region, the BL characteristic altered significantly, causing the fog layer to lift to low stratus cloud. The simulation and subsequent figures allowed for a unique vantage point of the evolution and mechanism that generated the fog within the YS region.

E. FOG STABILITY INDEX EVALUTION

The FSI is a commonly used index for fog forecasting throughout the AF community. The index is generated from a predetermined algorithm. The following equation is used in the upper-air model soundings to determine the likelihood of fog formation for a given area:

$$FSI = 2(T\text{-}Td) + 2(T – T850) + W850 \quad (1)$$

where T and Td are the air and dew-point temperature at 2 m (°C), T850 is the 850 mb air temperature, and W850 is the 850 mb wind speed in kts. The set of terms in equation (1), (T-Td), (T-T850), and W850 represent the humidity in the LL, the BL stability, and the wind speed above the BL at 850 mb, respectively (Holtslag *et al.* 2010). The output from this equation generates unit-less numerical values and through many research experiments, thresholds were determined. The following three thresholds describe the probability of fog formation: 1) high probability - FSI$\leq$31; 2) moderate probability - 31<FSI<55; 3) low probability - FSI $\geq$55.

Based on this FSI equation and the above thresholds, a comparison was conducted between the FSI values and the corresponding simulated q_c values at each point of interest. In addition, based on the results from a previous study by Holtslag, *et al.* (2010)

a modification to the coefficients was done which showed some improvement to the skill of the forecast index (Holtslag *et al.* 2010). Therefore, these modifications were applied to this sea fog case to determine if improvements in the FSI can be made. The results from this analysis are described in this section.

As shown in the previous result sections, the q_c values generated by the model accurately depicted the fog areas at each point of interest. Therefore, it is reasonable to consider the $q_c > 0.02$ $g \cdot kg^{-1}$ as fog. Thus, when producing a FSI based on the model output data and comparing it to the q_c, we should see a relatively close comparison between the two.

Figure 35 shows the time series analysis of the FSI (black lines) and the q_c at each point of interest. When FSI drops below 31 (dashed line), the probability for fog formation is high. Also, when q_c increases, the surface visibility also decreased at the given point. In other words, when the q_c increases, the FSI should decrease. Figure 35 shows that there is a close negative correlation between the two variables. However, it is noted that there are some differences. The ocean point (Figure 35a), which is experiencing fog for approximately 50 hours, shows a decrease in the FSI below 31 about 5 hours before the fog and 5 hours after the fog dissipated. This reflects an overforecast in the FSI in terms of the formation and dissipation of the fog. Also, when examining Kunsan and point L (Figure 35b/c), there's an obvious diurnal fluctuation occurring in the q_c and the FSI. However, the FSI at coastal location (Figure 35b) has a tendency of continuing the fog even during the day when no fog existed. While over the point L (Figure 35c), the FSI increase to above the high probability threshold value of 31. Perhaps the near coastal influences in the humidity and stability are driving the FSI to remain below the threshold values, while the farther onshore location has reduced in humidity and stability to drive the increase in the FSI values. Even though these comparisons are relatively accurate, there is some room for improvement.

The study conducted by Holtslag, *et al.,* (2010) compared the skill of the FSI based on observations near the Netherlands with the model output data from high resolution MM5 data. They also applied a correction in the coefficients to the original FSI algorithm to optimize the outcome of the FSI in various fog events. From the results,

a modified equation was developed and showed an increase in the accuracy of the fog forecast. The modification to the original FSI equation is as follows:

$$FSI = 21(T\text{-}Td) + 2(T – T850) + 0.5(W850) \quad (2)$$

The only changes to equation (1) were the coefficients associated with each of the main components: LL humidity, BL stability, and 850 mb wind speed (Holtslag *et al.* 2010). The large increase in the coefficient associated with the humidity factor indicates that there's a larger dependence on the saturation required for fog formation. While the decrease in the coefficient tied to the 850 mb winds in only a refelction of different units for wind speed used in the FSIs.

The calculated new FSI based on the modified equation is shown in Figure 36 in comparison with the model q_c at each point of interest (Figure 36). It was clear that there was improvements in accuracy of the index. The improvement in the FSI output shown in Figure 36, is shown on the outer bounds of the fog regions. For example, at point O (Figure 36a), there is no longer a period when the FSI indicated when the modeled q_c is nearly zero. Essentially, the timing of fog condition from the new FSI and from the cloud water matched nearly perfectly for each location. The only location that the FSI has a difficult time in forecast for the fog is at Kunsan AB (Figure 36b). Because of the coastal location, the model has a difficult time differentiating between the marine and land environments. This is in a way expected as all boundary layer parameterizations assumes horizontally homogeneous boundary layers. Nevertheless, the modified FSI shows promise in the realm of improving fog forecasting by the modification of the FSI to tighten the areas of inaccuracy.

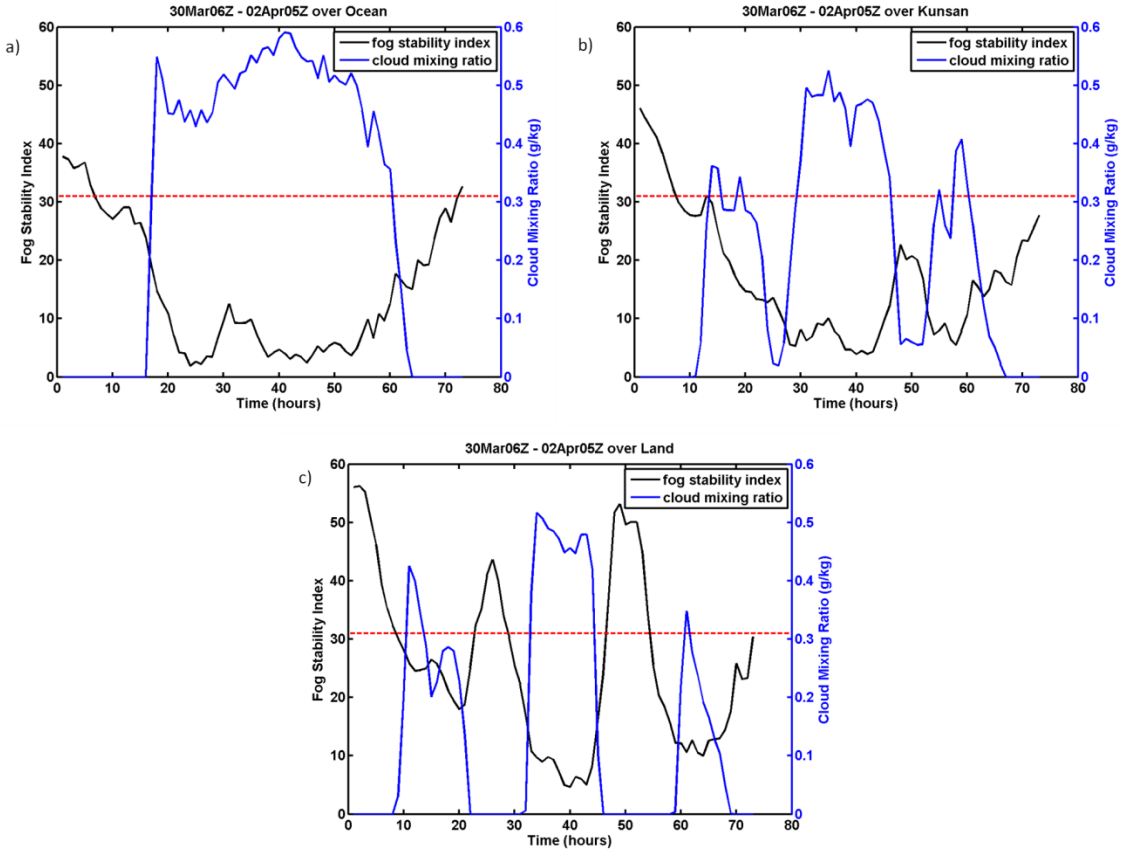

Figure 35. Time series analysis from the points of interest comparing the q_c from the generated FSI output. a) point O; b) Kunsan; c) point L. The red dashed line indicates the threshold between the high and moderate probability of fog. Below the line is high likelihood and above the line is moderate to low probability.

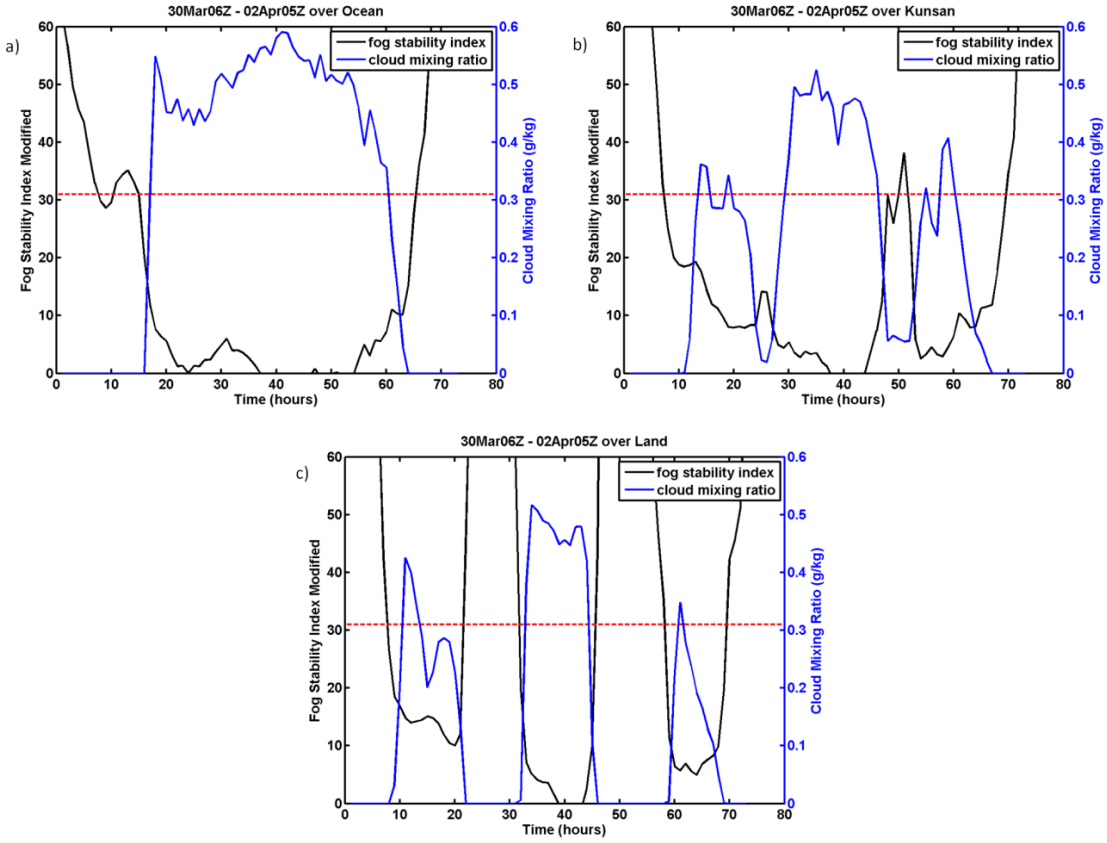

Figure 36. Time series analysis from the points of interest comparing the q_c from the generated FSI output using the modified equation. a) point O; b) Kunsan; c) point L. The red dashed line indicates the threshold between the high and moderate probability of fog. Below the line is high likelihood and above the line is moderate to low probability.

V. CONCLUSIONS, RECOMMENDATIONS, AND FUTURE RESEARCH

The overall objective of this thesis was to explore a case study of a sea fog event over the YS and to identify the relevant and essential physical processes that cause sea fog formation and dissipation. The intension of this analysis was to assist the 17 OWS and 8 OSS/OSW in finding a technique or ROT that could help reduce the inaccuracy of sea fog forecasts. Based on previous research, a concise description of advection sea fog was completed describing the essential processes that are required for its formation, sustainment, and dissipation. Due to the lack of available observational data, high resolution COAMPS model was used to simulate the fog event. A nested grid was constructed over the YS and ROK region with the innermost domain having 3 km horizontal grid resolution and 11 sigma levels up to 1600 m. Results analyzed in this study were generated from simulations from the innermost domain.

A comparison of the model accuracy to the observational data was made. It was concluded that the model simulation represented this fog event adequately. The only major discrepancy was in the duration of the fog period where the simulated fog extended beyond the dissipation of the observed fog. This may have to do with the model physics in the radiation scheme that overestimated the cloud-top radiative cooling. This effect causes significant reduction in near-surface temperature compared to the limited amount of observations and is considered a factor in the prolonged fog period in the model.

The methods used in this study were to examine the development of sea fog along a trajectory of an air column arriving at three separate locations: over the sea, over Kunsan AB (coastal region), and over land. To follow the different air columns, back trajectory analyses were conducted from the initial period of fog formation at each location. Along the air trajectories, contour plots of various boundary layer variables and surface properties were generated to show the effects of air-sea interaction in the development of fog. To investigate the sustainment of fog, a time series analysis for the entire model period was completed to observe the evolution of the fog layer at each individual location. Additionally, spatial variability was examined through analyses of a

vertical cross-section cutting through each of the three points of interest at different stages of the life cycle of this fog event throughout the model run. Finally, a comparison of the modeled q_c and the widely-used FSI was completed to see how well the index performed in forecasting this particular event. This analysis yielded a suggested modification to the original FSI formulation which ultimately led to a more accurate comparison between the FSI and the modeled fog event as indicated by the q_c values. This result is consistent with those from a recent study conducted by Holtslag, *et al.*, (2010).

This sea fog event at Kunsan had characteristics of both land based radiation fog and advection sea fog. In fact, as described in chapter 2, the initial period of the fog formation appeared to be an advection-radiation fog, where the combination of the advection of warm, moist air and the radiative cooling of the land surface generated the fog. Shortly after the fog over land initially formed during the night hours on 30 March, it started to develop over the water near the coast in regions with the nighttime presence of fog. It is possible that this fog over the sea was advected due to the weak easterly wind in the nighttime fog region overland. However, the sea fog extended over a much larger region to the west with time. Throughout the next day, the fog was maintained over the sea. Kunsan experienced fog on the following evening. Unlike the previous night, the fog layer at Kunsan had about the same depth as that in the adjacent sea. It appears this fog at Kunsan on the second night was part of the sea fog advected overland. This hypothesis is consistent with development of the sea breeze circulation discussed earlier. This case study showed that due to the difference in the surface characteristics between the land and sea, fog is able to have a longer lifecycle over the sea. However, when the land cools, the moisture remains abundant and the synoptic pattern persists, the fog is capable of flowing from the sea to the land.

Through the series of analyses, some common characteristics were uncovered for fog development and dissipation. The wind speed and direction was a major contributing factor in the life cycle of fog. In all of the figures, a persistent west-southwesterly flow dominated the region. This wind field was a result of the LL high pressure system that was situated over the southern part of the YS. This flow pattern enabled the influx of

warm, moist air from the tropical region in the ECS to the YS and west coast of ROK. The high pressure also generated an increase in the subsidence, which contributed to the LL inversion above the MABL. Also, immediately after fog formation at each location the BL height dropped rapidly. Although radiative cooling resulted in significant temperature drop in the fog layer, it does not seem to generate much turbulent mixing within the fog. This is partly due to the strong static stratification in the lowest 50 m of the atmosphere due to strong near surface cooling. It is also possible that the shallow fog layer does not allow the full development of turbulence as radiative cooling happens nearly within the entire layer.

Another important general characteristic was the air-sea interaction that was taking place prior to fog formation. The surface SHF suggested heat input from the atmosphere to the sea surface before fog formed along most of the trajectory. This trend continued until the air temperature decreased to below the SST immediately before fog formation. While on the other hand, the LHF from the sea surface was primarily positive, indicating an upward flux of moisture which contributed to the increase in q_v throughout the trajectory. However, when the trajectory tracked over the land the fluxes showed dramatic differences in magnitude consistent large air-surface temperature differences.

The time series analyses at each point also showed some variations based on the life span of the fog. Over the ocean the fog was sustained for over 40 hours when the temperature of the BL remained below the SST. In addition, the SHF/LHF remained relatively low and positive to keep supplying moisture from the ocean surface. However, over the land surfaces, the fog regions along with the associated fluxes displayed strong diurnal variations. The daytime heating period led to SHF and LHF values above 300 and 200 $W \cdot m^{-2}$, respectively. These large surface fluxes did not result in a deeper boundary layer as further inland, but they were rather effective in dissipating the fog during the day.

The dissipation of the sea fog in this study occurred because of the change in the large scale synoptic pattern. A synoptic frontal boundary from the north modified the LL environment to the extent that it was unable to support a moist and stable BL. The dry

and strong winds (> 40 kts) mixed out LL fog by lifting the BL height and evaporating fog liquid water. This type of air modification is a common reason for fog dissipation in the region.

This thesis work re-evaluated the FSI for fog forecasting. The original FSI is capable of producing a broad fog period, but lacks the accuracy in the starting and ending of the fog event. Some of the limiting factors of the FSI were also discussed in Chapter 4. An attempt was made to use newly developed FSI algorithms found in the literature. Refined fog forecast were done using the new FSI.

Even though the results from this analysis revealed some general characteristics in the fog formation, maintenance, and dissipation processes, they represent only a small sample of the sea fog events throughout the year. A more thorough analysis is needed that requires similar analyses with a substantial amount of cases. It is hence important to maintain an accurate and substantial data archive for fog events. The ability to examine various types of sea fog events over multiple fog seasons is crucial for diagnosing the particular criteria for sea fog development and developing an adequate ROT. Also, due to the fact that the observation system within the YS is scarce, it becomes difficult to evaluate ever-evolving sea surface characteristics. Therefore, understanding the ocean currents and tidal influences associated with the YS can lead to a clearer picture of the thermal structure of the sea during the fog season. Coupled atmosphere and ocean simulations may provide more insight to the fog development processes as shown in recent study by Heo and Ha (2010), and should be the focus of future studies.

The modified FSI may be a useful correction to the immediate problem, but its application may be limited to certain conditions and regions. Therefore, it is recommended to the 17 OWS to save data during all sea fog events within the YS in order to gain an accurate picture of all the physical processes surrounding the development of a plethora of fog formations in the region throughout the year. Also, taking the approaches used in this thesis to examine the sea fog characteristics is an additional benefit for creating a long term solution to this continuous problem.

LIST OF REFERENCES

AFCCC, 2005: Operational Climatic Data Summary (OCDS), Kunsan AB, Korea.

Air Force Manual (AFMAN) 15–111, 2009: Surface Weather Observations, HQ AFWA/XOW.

Apel, J., 2004: Yellow Sea. *Global Ocean Ass., Off. of Naval Res.* 425–432.

Cho, Y.K., M.O. Kim, and Q.C. Kim, 2000: Sea Fog around the Korean Peninsula. *Jour. of App. Met. and Climatology*, **39.12**, 2473–2479.

Cummings, J.A., 2005: Operational multivariate ocean data assimilation. *Quart. J. Royal Met. Soc.*, **Part C-131(613)**, 3583-3604.

Dalu, G.A., and M. Baldi, 2003: Mesoscale Nonhydrostatic and Hydrostatic Pressure Gradient Forces-Theory. *Jour. of Atm. Sci.*, **60.18**, 2249–2266.

Gao, S., H. Lin, B. Shen, and G. Fu, 2007: A Heavy Sea Fog Event over the Yellow Sea in March 2005: Analysis and Numerical Modeling. *Adv. in Atm. Sci.*, **24.1**, 65–81.

Giese, P., 2004: Korea — A Full Year Study. *Air Force Combat Climatology Center*, **AFCCC/CD-04/01**, 1–80.

GlobalSecurity.org, cited 2011: Kunsan Air Base summary. [Available online at http://www.globalsecurity.org/military/facility/kunsan.htm.]

Gultepe, I., and Coauthors, 2007: Fog Research: A Review of Past Achievements and Future Perspectives. *Pure & App. Geophysics*, **164.6-7**, 1121–1159

Heo, K.Y., and K.J. Ha, 2010: A Coupled Model Study on the Formation and Dissipation of Sea Fogs. *Mon. Wea. Rev.*, **138.4**, 1186–1204.

Holtslag, M.C., G.J. Steeneveld, and A.A.M. Holtslag, 2010: Fog forecasting: "old fashioned" semi-empirical methods from radio sounding observations versus "modern" numerical models. *5th International Conference on Fog, Fog Collection and Dew*, FOGDEW2010-69.

Kochi University, Japan, Weather Home, cited 2011: GMS/GOES9/MTSAT Data Archive for Research and Education. [Available at http://weather.is.kochi-u.ac.jp/sat/JPN/2011/.]

Koracin, D., J.A. Businger, C.E. Dorman, and J.M. Lewis, 2005: Formation, Evolution, and Dissipation of Coastal Sea Fog. *Boundary-Layer Met.*, **117–3**, 447–478.

Korean Meteorological Agency, cited 2011: Buoy data for Chilbaldo. [Available at http://www.kma.go.kr/weather/observation/marine_buoy.jsp?type=time&x=14&y=9&stn=22102&tm=2011.04.1.10.]

Kunkel, B. A., 1984: Parameterization of droplet terminal velocity and extinction coefficient in fog models. *J. Climate Appl. Meteor.*, **23**, 34–41.

Lewis, D., Capt, 2004: Forecasting Advection Sea Fog with the Use of Classification and Regression Tree Analyses for Kunsan Air Base. M.S. thesis, Department of Meteorology, Air Force Institute of Technology, 103 pp.

Mask, A., and J. O'Brien, 1998: Wind-driven effects on the Yellow Sea Warm Current. *Jour. of Geophys. Res.*, **103-C13**, 30, 71–30, 729.

Microsoft Corp., cited 2011: Bing Maps of Korean Peninsula. [Available at http://www.bing.com/maps/.]

Noone, D., and I. Simmonds, 1999: A three-dimensional spherical trajectory algorithm. Research Activities in Atmospheric and Oceanic Modeling, Report No. 28, WMO/TD-No. 942. H. Ritchie, Ed., *World Met. Org.*, **3.26-3.27**.

NRL/Marine Meteorology Division 2003, cited 2011: COAMPS Version 3 Model Description: General Theory and Equations. [Available at http://www.nrlmry.navy.mil/coamps-web/web/view.]

Republic of Korea Air Force (ROKAF), cited 2011: Analyzed weather maps surface and 500 mb for 30 March 2011 – 02 April 2011.

Roach, W.T., 1995: Back to Basics: Fog: Part 3: The Formation and Dissipation of Sea Fog. *Wea., Bracknell, England*, **50.3**, 80–84.

University of Wyoming, College of Engineering, Department of Atmospheric Science, cited 2011: Upper air sounding data for Kwangju AB, Korea. [Available at http://weather.uwyo.edu/upperair/sounding.html.]

Wang, B., 1985: *Sea Fog*. China Ocean Press, 330 pp.

Wikipedia.org, cited 2011: South Korea Topography image. [Available at http://en.wikipedia.org/wiki/File:South_Korea_Topography.png.]

Zhang, S.P., S.P. Xie, Q.Y. Liu, Y.Q. Yang, X.G. Wang, and Z.P. Ren, 2009: Seasonal Variations of Yellow Sea Fog: Observations and Mechanisms. *Jour. of Climate.*, **22.24**, 6758–6772.

Zhou, B., and J. Du, 2010: Fog Prediction from a Multimodel Mesoscale Ensemble Prediction System. *Wea. and Fore.*, **25.1**, 303–322.

THIS PAGE INTENTIONALLY LEFT BLANK

INITIAL DISTRIBUTION LIST

1. Defense Technical Information Center
   Ft. Belvoir, Virginia

2. Dudley Knox Library
   Naval Postgraduate School
   Monterey, California

3. Dr. Qing Wang
   Naval Postgraduate School
   Monterey, California

4. Dr. Wendell A. Nuss
   Naval Postgraduate School
   Monterey, California

5. Dr. Shouping Wang
   Naval Research Laboratory
   Monterey, California

6. 17th Operational Weather Squadron
   Hickam AB, Hawaii

7. 8th Operations Support Squadron, Weather Flight
   Kunsan AB, Republic of Korea

8. Air Force Weather Technical Library
   Asheville, North Carolina